

An alternative approach to train neural networks using monotone variational inequality

Chen Xu^{*1}, Xiuyuan Cheng^{†2}, and Yao Xie^{‡1}

¹H. Milton Stewart School of Industrial and Systems Engineering, Georgia Institute of Technology.

²Department of Mathematics, Duke University

Abstract

Despite the vast empirical success of neural networks, theoretical understanding of the training procedures remains limited, especially in providing performance guarantees of testing performance due to the non-convex nature of the optimization problem. The current paper investigates an alternative approach of neural network training by reducing to another problem with convex structure — to solve a monotone variational inequality (MVI) - inspired by a recent work of (Juditsky & Nemirovsky, 2019). The solution to MVI can be found by computationally efficient procedures, and importantly, this leads to performance guarantee of ℓ_2 and ℓ_∞ bounds on model recovery and prediction accuracy under the theoretical setting of training a single-layer linear neural network. In addition, we study the use of MVI for training multi-layer neural networks and propose a practical algorithm called *stochastic variational inequality* (SVI), and demonstrate its applicability in training fully-connected neural networks and graph neural networks (GNN) (SVI is completely general and can be used to train other types of neural networks). We demonstrate the competitive or better performance of SVI compared to widely-used stochastic gradient descent methods on both synthetic and real network data prediction tasks regarding various performance metrics, especially in the improved efficiency in the early stage of training.

1 Introduction

Neural network (NN) training (Duchi et al., 2010; Sutskever et al., 2013; Kingma & Ba, 2015; Ioffe & Szegedy, 2015a) is the essential process in the study of deep models. Optimization guarantee for training loss as well as generalization error have been obtained with over-parametrized networks (Neyshabur et al., 2014; Mei et al., 2018; Arora et al., 2019a,b; Allen-Zhu et al., 2019; Du et al., 2019). However, due to the inherent non-convexity of loss objectives, theoretical developments are still diffused and lag behind the vast empirical successes.

*cxu310@gatech.edu

†xiuyuan.cheng@duke.edu

‡yao.xie@isye.gatech.edu

Recently, the seminal work (Juditsky & Nemirovsky, 2019) presented a somehow surprising result that some non-convex issues can be circumvented in special cases by problem reformulation. In particular, it was shown that when estimating the parameters of the generalized linear models (GLM), instead of minimizing a least-square loss function, which leads to a non-convex optimization problem, and thus no guarantees can be obtained for global convergence nor model recovery, one can reformulate the problem as solving an monotone variational inequality (MVI), a general form of convex optimization. The reformulation through MVI leads to strong performance guarantees and computationally efficient procedures.

In this paper, inspired by (Juditsky & Nemirovsky, 2019) and the fact that certain GLM (such as logistic regression) can be viewed as the simplest neural network with only one layer, we consider a new scheme for neural network training based on MVI. This is a drastic departure from the widely used gradient descent algorithm for neural network training — we replace the gradient of a loss function with a carefully constructed monotone operator. The benefits of such an approach include (i) in special cases (one input layer networks), we can establish strong training and prediction guarantees – see Section 4; (ii) for general cases, through extensive numerical studies on synthetic and real-data in Section 5, we demonstrate the faster convergence to a local solution by our approach relative to gradient descent in a comparable setup.

To the best of our knowledge, the current paper is the first to study MVI for training neural networks. Our SVI, as a general way of modifying the parameter update scheme in NN training, can be readily applied to various deep architectures. In this work, beyond fully-connected (FC) neural networks, we especially study MVI training for node classification in graph neural networks (GNN) (Wu et al., 2019; Pilanci & Ergen, 2020), due to the ubiquity of network data and the importance of network prediction problems. Specifically, our technical contributions include:

- Develop a heuristic algorithm called *stochastic variational inequality* (SVI) for training multi-layer neural networks. In particular, the algorithm provides a fundamentally different but easy-to-implement alternative to using gradient during training.
- Reformulate the single/last-layer neural network training as solving a monotone variational inequality, with guarantees on recovery and prediction accuracy.
- Compare SVI with widely-used stochastic gradient descent methods to demonstrate the competitiveness of SVI, especially the improved efficiency in the early stage of training.

Literature. MVI has been studied in priors mainly in the optimization problem context (Kinderlehrer & Stampacchia, 1980; Facchinei & Pang, 2003), which can be viewed as the most general problems with convex structure (Juditsky & Nemirovski, 2021). More recently, VI has been used to solve min-max problems in Generative Adversarial Networks (Lin et al., 2018) and reinforcement learning (Kotsalis et al., 2020). In particular, our theory and techniques are inspired by (Juditsky & Nemirovsky, 2019), which uses strongly monotone VI for signal recovery in generalized linear models (GLM). In contrast to their work, we offer a thorough investigation of using VI to train multi-layer NN and address the case when VI may not be strongly monotone. On the other hand, we emphasize the difference from (Pilanci & Ergen, 2020), which views two-layer NNs as convex regularizers: we focus on model recovery rather than change variables to convexify the loss minimization. In addition, our SVI extends beyond two-layer networks.

The rest of the work proceeds as follows. Section 2 describes the general NN and GNN models we tackle and provides preliminaries of MVI. Section 3 provides the SVI algorithm for training one-layer and multi-layer neural networks. Section 4 presents various theoretical guarantees, including the model recovery recovery guarantees measured in ℓ_p error. We also emphasize cases where the MVI training is identical to gradient-based methods and when the graph is estimated in GNN models. Section 5 compares SVI and the stochastic gradient descent (SGD) on various synthetic and real-data examples to illustrate the potential benefits of SVI. Section 6 concludes the paper. Appendix A contains proofs and B contains various additional experiment results.

2 Problem setup

We first introduce the general neural network model in Section 2.1 and then specify the class of graph neural networks (GNN) we can tackle in Section 2.2, after which the MVI preliminaries are introduced in Section 2.3.

2.1 Notation of general NN

Assume a generic feature $X \in \mathbb{R}^C$, where C denotes the feature dimension. Suppose the conditional expectation $\mathbb{E}[Y|X]$ of the categorical response vector¹ $Y \in \{1, \dots, K\}$ is modeled by an L -layer neural network $f(X, \Theta)$:

$$\mathbb{E}[Y|X, \Theta] := f(X, \Theta) = \phi_L(g_L(X_L, \Theta_L)), \quad (1)$$

where $X_L = \phi_{L-1}(g_{L-1}(X_{L-1}, \Theta_{L-1}))$, $X_1 = X$ denote the nonlinear feature transformation from the previous layer, $\Theta = \{\Theta_1, \dots, \Theta_L\}$ denotes model parameters, and each ϕ_l denotes the activation function at layer l . In particular, assume there exists $\Theta^* = \{\Theta_1^*, \dots, \Theta_L^*\}$ so that $\mathbb{E}[Y|X] = f(X, \Theta^*)$.

The goal is to estimate parameters Θ^* using N training data, with performance guarantee on bounding the error between the final predictor $f(X_t, \hat{\Theta})$ and the ground truth $f(X_t, \Theta^*)$, $t > N$. In particular, we would consider the ℓ_p error $\|f(X_t, \hat{\Theta}) - f(X_t, \Theta^*)\|_p$. To this end, we adopt monotone variational inequality (MVI) for training in Section 3. In particular, we will cast the one-layer training as solving an MVI in Section 3.1 and present a practical algorithm motivated by MVI to train parameters in all layers in Section 3.2.

2.2 Notation of GNN models

We first introduce the basics of graph filtering and then specify a class of filters that our MVI method to be proposed in Section 3 can handle. It should be understood that our techniques can be applied for general neural network training (e.g., networks in (1)). Experiments for both FC networks and GNN appear in Section 5.

Suppose we have an undirected and connected graph $\mathcal{G} = (\mathcal{V}, \mathcal{E}, W)$, where \mathcal{V} is a finite set of n vertices, \mathcal{E} is a set of edges, and $W \in \mathbb{R}^{n \times n}$ is a weighted adjacency matrix encoding node connections. Let I_n

¹The techniques and theory in this work can be used to model the conditional expectation of continuous random variables.

denote an identity matrix of size n . Let D be the degree matrix of W and $L_g = I_n - D^{-1/2}WD^{-1/2}$ be the normalized graph Laplacian, which has the eigendecomposition $L_g = U\Lambda U^T$. For a graph signal $X \in \mathbb{R}^{n \times C}$ with C input channels, it is then filtered via a function $g_\Theta(L_g)$ which acts on L_g with channel-mixing parameters $\Theta \in \mathbb{R}^{C \times F}$ for F output channels. Thus, the filtered signal $X' = g_\Theta(L_g)X$.

Our MVI framework to be introduced next can handle a class of graph filters in which the filter and parameter are *decoupled* before applying the activation function. For instance, for some positive integer R , $g_\Theta(L_g)X = \sum_{r=1}^R g_r(L_g)X\Theta_r$, where $g_r(L)$ is fixed (non-adaptive) graph filters determined by graph Laplacian, and Θ_r is trainable parameters. Note that this class of filters include some popular ones:

- *Graph Convolutional Network (GCN)* (Kipf & Welling, 2017):

$$g_\Theta(L_g)X = (\tilde{D}^{-\frac{1}{2}}\tilde{W}\tilde{D}^{-\frac{1}{2}})X\Theta,$$

where $\tilde{W} := W + I_n$ is the graph with self-loops.

- *Chebyshev Network (Chebnet)* (Defferrard et al., 2016):

$$g_\Theta(L_g)X = \sum_{k=1}^K T_k(L_g)X\Theta_k,$$

for the K^{th} -order Chebyshev polynomials $\{T_1, \dots, T_K\}$.

- *Graph Sample and Aggregate (GraphSAGE)* (Hamilton et al., 2017):

$$[g_\Theta(L_g)X]_i = \Theta_1 x_i + \text{mean}_{j \in N(i)} x_j.$$

More generally, our framework works as long as that there exists a mapping η such that

$$g_\Theta(L_g)X = \eta(X)\Theta. \quad (2)$$

2.3 Preliminaries of MVI

We now introduce the notion of MVI and discuss the problem computability, where concrete training techniques are presented in Section 3. Given a parameter set $\Theta \subset \mathbb{R}^p$, we call a continuous mapping (operator) $F : \Theta \rightarrow \mathbb{R}^p$ *monotone* if for all $\Theta_1, \Theta_2 \in \Theta$, $\langle F(\Theta_1) - F(\Theta_2), \Theta_1 - \Theta_2 \rangle \geq 0$. (Juditsky & Nemirovsky, 2019) The operator is called *strongly monotone* with modulus κ if for all $\Theta_1, \Theta_2 \in \Theta$,

$$\langle F(\Theta_1) - F(\Theta_2), \Theta_1 - \Theta_2 \rangle \geq \kappa \|\Theta_1 - \Theta_2\|_2^2. \quad (3)$$

If $F \in C^1(\Theta)$ (i.e., continuously differentiable on Θ) and Θ is closed and convex with non-empty interior, (3) holds if and only if $\lambda_{\min}(\nabla F(\Theta)) \geq \kappa$ for all $\Theta \in \Theta$, where $\lambda_{\min}(\cdot)$ denotes the minimum eigenvalue of a square matrix.

Now, for a monotone operator F on Θ , the problem $\text{VI}[F, \Theta]$ is to find an $\bar{\Theta} \in \Theta$ such that for all

$\Theta \in \Theta$,

$$\langle F(\bar{\Theta}), \Theta - \bar{\Theta} \rangle \geq 0. \quad \text{VI}[F, \Theta]$$

It is known that if Θ is compact, then $\text{VI}[F, \Theta]$ has at least one solution (Oustrata et al., 2013, Theorem 4.1). In addition, if $\kappa > 0$ in (3), then $\text{VI}[F, \Theta]$ has exactly one solution (Oustrata et al., 2013, Theorem 4.4). Under mild computability assumptions, the solution can be efficiently solved to high accuracy, using various iterative schemes (with a similar form as stochastic gradient descent or accelerated gradient descent by replacing the gradient by the monotone operator) (Juditsky & Nemirovsky, 2019).

3 MVI for neural network training

We now present the MVI-based algorithms for training neural networks. We start with simple one-layer network training with MVI, where the framework and techniques directly come from (Juditsky & Nemirovsky, 2019), and highlight the similarity/difference with the standard stochastic gradient descent (SGD). We then generalize to training multiple-layer neural networks.

3.1 One-layer neural network training

Let us first consider training a one-layer neural network (i.e., $L = 1$ in (1)) with a particular form of pre-activation: $g(X, \Theta) = \eta(X)\Theta$ for an arbitrary feature transformation η . In the simplest case for fully connected neural networks $\eta(X) = X$, i.e., the identity map. In the GNN case, as in (2), it is the filtered signal before multiplying with the channel-mixing coefficients Θ . Note that in this special case, the training of neural network is mathematically equivalent to the estimation of a GLM with properly chosen activation function Juditsky & Nemirovsky (2019).

We construct the monotone operator F as

$$F(\Theta) := \mathbb{E}_{X,Y} \{ \eta^\top(X) [\phi(\eta(X)\Theta) - Y] \}, \quad (4)$$

where $\eta^\top(X)$ denotes the transpose of $\eta(X)$. We will explain a few properties of F in Sec. 4, Lemma 4.1. Given training samples, we can form an empirical sample version of F denoted by \hat{F} . Then the training based on MVI

$$\Theta \leftarrow \text{Proj}_\Theta(\Theta - \gamma \hat{F}(\Theta)). \quad (5)$$

where $\gamma > 0$ is the step-size, Proj_Θ denotes the projection operation to ensure the updated parameters are still within feasible parameter domain Θ .

Note that (5) differs from SGD where the gradient of a certain loss objective takes the role of the monotone operator \hat{F} . In particular, \hat{F} does not need to correspond to the gradient of any loss function. Nevertheless, we will show in Section 4.3, Proposition 4.7 that \hat{F} is exactly the gradient of the cross-entropy loss with respect to parameter Θ if ϕ is either the sigmoid or softmax, whereby (5) coincides with SGD.

3.2 Multi-layer neural network training

Based on our one-layer training framework, we require the general model (1) to take the form that for each $l \leq L$,

$$g_l(X_l, \Theta_l) = \eta_l(X_l)\Theta_l, \quad (6)$$

where η_l is the nonlinear feature transformation in layer l , which can differ over layers. Based on Section 3.1, it is natural to replace the gradient of the objective with respect to Θ_l by $F_l(\Theta_l)$ in (4), where Y is replaced by Y_l such that $\mathbb{E}[Y_l|X] = \phi_l(\eta_l(X_l)\Theta_l)$, so that dimensions match.

Unfortunately, Y_l implicitly depends on the true parameters in all previous layers, which are never known, so this naive approach fails. Instead, we provide a heuristic *stochastic variational inequality* (SVI) in Algorithm 1, which is motivated by both MVI in the one-layer training training and the traditional empirical loss minimization. In the algorithm, $X_{i,l}^t$ is the hidden representation of X_i using parameter estimates at the t^{th} iteration in all previous layers, denoted as $\hat{\Theta}_{1:l-1}^t$. Meanwhile, $f(X_{j,l+1}^t, \hat{\Theta}_{l+1:L}^t) = f(X_j, \hat{\Theta}^t)$ is the output of the neural network from layer $l+1$ onward.

Algorithm 1 Stochastic variational inequality (SVI).

Require: Inputs are (a) Training data $\{(X_i, Y_i)\}_{i=1}^N$, batch number B , and epochs E ; (b) An L -layer network $f(X, \Theta) := \{\phi_l(g_l(X_l, \Theta_l))\}_{l=1}^L$; (c) Initial parameters $\hat{\Theta}_{1:L}^0 := \{\hat{\Theta}_l^0\}_{l=1}^L$; (d) Loss function $\mathcal{L}(f(X, \Theta), Y)$.

Ensure: Estimated parameters $\hat{\Theta}^T$, $T := \lceil NE/B \rceil$

- 1: Let $I := \lceil N/B \rceil$ be the number of iterations per epoch and denote batches as b_1, \dots, b_I .
 - 2: **for** epoch $e = 0, \dots, E$ and iteration $i = 1, \dots, I$ **do**
 - 3: Compute $t := eI + i$ as the current iteration index
 - 4: Compute gradient simultaneously at each layer l as:
 - 5: **If** $l < L$

$$F_l^t := b_i^{-1} \sum_{j \in b_i} \eta^\top(X_{j,l}^t) \nabla_{X_{j,l+1}^t} \mathcal{L}(f(X_{j,l+1}^t, \hat{\Theta}_{l+1:L}^t), Y_j)$$
 - 6: **If** $l = L$

$$F_L^t := b_i^{-1} \sum_{j \in b_i} \eta^\top(X_{j,L}^t) [\phi_L(\eta(X_{j,L}^t)\hat{\Theta}_L) - Y_j]$$
 - 7: Update $\hat{\Theta}_l^{t+1}$ according to (5) using F_l^t , where one may incorporate acceleration techniques.
 - 8: **end for**
-

We briefly justify line 5 in Algorithm 1, which is the heuristic step in previous layers. For instance, let $\mathcal{L}(f(X_{l+1}, \Theta_{l+1:L}), Y)$ be the MSE loss and note that

$$\nabla_{X_{l+1}} \mathcal{L}(f(X_{l+1}, \Theta_{l+1:L}), Y) = [f(X_{l+1}, \Theta_{l+1:L}) - Y] \nabla_{X_{l+1}} f(X_{l+1}, \Theta_{l+1:L}),$$

which can be computed via backpropagating the loss on *hidden layer outputs* X_{l+1} rather than on the *model parameter* Θ_l ; $F_l(\Theta_l)$ is then formed by mapping the gradient back to the parameter space, similar as (4). However, we cannot verify that $F_l(\Theta_l)$ is monotone in Θ_l , even if parameters in later layers are fixed. In fact, we suspect monotonicity in all layers is impossible, as this would make the non-convex multi-layer neural network training convex without any relaxation.

Remark 3.1 (Effect on training dynamics). We remark a key difference between the gradient update in vanilla

stochastic gradient descent (SGD) and that in SVI, which ultimately affects training dynamics. Suppose the activation function at layer l is ReLU, so $X_{l+1} = \text{ReLU}(\eta(X_L^*)\Theta_l^*)$. Under the MSE loss, we notice that for SGD:

$$\nabla_{\Theta_l} \mathcal{L} = [f(X_{l+1}, \Theta_{l+1:L}) - Y] \nabla_{\Theta_l} \text{ReLU}(\eta(X_L^*)\Theta_l),$$

and for SVI:

$$\nabla_{X_{l+1}} \mathcal{L} = [f(X_{l+1}, \Theta_{l+1:L}) - Y] \nabla_{X_{l+1}} f(X_{l+1}, \Theta_{l+1:L}).$$

In particular, SGD does not update weights of inactive neurons because the gradient of ReLU with respect to them is zero. However, SVI does not discriminate between these neurons as the gradient is taken with respect to *outputs* from the current layer. Thus, one can expect that SVI results in further weight updates than SGD, which experimentally seem to speed up the initial model convergence. We illustrate this phenomenon in Figure 3 and will provide explanations in future works.

4 Guarantee of model recovery by MVI

We now present guarantees on model recovery for the *last-layer training* when previous layers are fully known; in practice, this can be understood as if previous layers have provided necessary feature extraction. This guarantee naturally hold in one-layer networks. In particular, we provide pointwise (resp. in expectation) error bound on predicting $\mathbb{E}[Y_t|X_t]$ in Section 4.1 (resp. Section 4.2), where κ in (3) satisfies $\kappa > 0$ (resp. $\kappa = 0$) for the strongly monotone (resp. monotone) VI. In addition, we discuss in Section 4.3 when the monotone operator F in (4) is exactly the expectation of the gradient of model parameters; guarantees thus hold for gradient-based methods in such cases. Lastly, we also consider imprecise graph knowledge in Section 4.4. We remark that guarantees in Section 4.1, 4.2, and 4.3 hold as long as $\mathbb{E}[Y|X] = \phi(\eta(X)\Theta)$, which encompasses both FC networks and certain classes of GNN models mentioned earlier in Section 2.

Let $\{(X_i, Y_i)\}_{i=1}^N$ be N training data from model (1) with $\Theta = \Theta^*$. For the subsequent theoretical analyses, we assume that for each i , the quantity $X_{i,L}^*$ is known, which is the output from the previous $L - 1$ hidden layers using X_i and the true parameters $\{\Theta_1^*, \dots, \Theta_{L-1}^*\}$. Thus, $\eta(X)$ becomes $\eta(X_L^*)$ for a generic feature X . For the operator $F(\Theta_L)$ in (4), where Θ is the parameter space of Θ_L , consider its empirical average $F_{1:N}(\Theta_L) := (1/N) \sum_{i=1}^N F_i(\Theta_L)$, where $F_i(\Theta_L) := \eta^\top(X_{i,L}^*)[\phi(\eta(X_{i,L}^*)\Theta_L) - Y]$. Let $\hat{\Theta}_L^{(T)}$ be the estimated parameter after T training iterations, using $F_{1:N}$ and (5). For a test feature X_t and its nonlinear transformation $X_{t,L}^*$, consider

$$\hat{\mathbb{E}}[Y_t|X_t] := \phi_L(\eta(X_{t,L}^*)\hat{\Theta}_L^{(T)}), \quad (7)$$

which is the estimated prediction using $\hat{\Theta}_L^{(T)}$ and will be measured against the true model $\mathbb{E}[Y_t|X_t]$ under Θ_L^* . In particular, we will provide error bound on $\|\hat{\mathbb{E}}[Y_t|X_t] - \mathbb{E}[Y_t|X_t]\|_p, p \geq 2$ which crucially depends on the strong monotonicity modulus κ in (3) for $F(\Theta_L)$.

We first state a few properties of $F(\Theta_L)$ defined in (4), which explicitly identify the form of κ . All proofs of Lemmas and Theorems are contained in Appendix A.

Lemma 4.1. Assume ϕ_L is K -Lipschitz continuous and monotone on its domain. For a generic input X ,

1. $F(\Theta_L)$ is both monotone and K_2 -Lipschitz, where $K_2 := K\mathbb{E}_X\{\|\eta(X_L^*)\|_2^2\}$.
2. $\kappa = \lambda_{\min}(\nabla\phi_L)\mathbb{E}_X[\lambda_{\min}(\eta^\top(X_L^*)\eta(X_L^*))]$ if $\nabla\phi_L$ exists; it is 0 otherwise.
3. $F(\Theta_L^*) = 0$.

For simplicity, we assume from now on the stronger condition that $\lambda_{\min}(\eta^\top(X_L^*)\eta(X_L^*)) > 0$ for any generic nonlinear feature X_L^* . In addition, because we are considering the last layer in classification, ϕ_L is typically chosen as sigmoid or softmax, both of which are differentiable so $\lambda_{\min}(\nabla\phi_L)$ exists. Note the property $F(\Theta_L^*) = 0$ implies that Θ_L^* is a solution to $\text{VI}[F, \Theta]$. In particular, if $\kappa > 0$, it is the *unique* solution. As a result, Θ_L^* can be efficiently solved to a high accuracy using $F(\Theta_L)$ under appropriated chosen γ in (5).

4.1 Case 1: modulus $\kappa > 0$

Under appropriate selection of step size and additional assumptions, we can obtain bounds on the recovered parameters following techniques in (Juditsky & Nemirovsky, 2019), which helps us to bound the error in model recovery and prediction. Note that the guarantee relies on the value κ , which may be approximated by the empirical average using N training data.

Lemma 4.2 (Parameter recovery guarantee). *Suppose that there exists $M < \infty$ such that $\forall \Theta_L \in \Theta$,*

$$\mathbb{E}_{X, Y^{\Theta_L}} \|\eta(X_L^*)Y^{\Theta_L}\|_2 \leq M,$$

where $\mathbb{E}[Y^{\Theta_L}|X] = \phi(\eta(X_L^*)\Theta_L)$. Choose adaptive step sizes $\gamma = \gamma_t := [\kappa(t+1)]^{-1}$ in (5). The sequence of estimates $\widehat{\Theta}_L^{(T)}$ obeys the error bound

$$\mathbb{E}_{\widehat{\Theta}_L^{(T)}} \{\|\widehat{\Theta}_L^{(T)} - \Theta_L^*\|_2^2\} \leq \frac{4M^2}{\kappa^2(T+1)}. \quad (8)$$

We can use the above result to bound the error in posterior prediction.

Theorem 4.3 (Prediction error bound for model recovery, strongly monotone F). *We have for a given test signal $X_t, t > N$ that for $p \in [2, \infty]$,*

$$\mathbb{E}_{\widehat{\Theta}_L^{(T)}} \{\|\widehat{\mathbb{E}}[Y_t|X_t] - \mathbb{E}[Y_t|X_t]\|_p\} \leq (T+1)^{-1}C_t,$$

where $C_t := [4M^2K\lambda_{\max}(\eta^\top(X_{t,L}^*)\eta(X_{t,L}^*))]/\kappa^2$ and $\widehat{\mathbb{E}}[Y_t|X_t]$ is defined in (7). In particular, $p = 2$ yields the sum of squared error bound on prediction and $p = \infty$ yields entry-wise bound (over the graph nodes).

Note that the guarantee is point-wise, as we are able to bound the parameter recovery error in expectation in Lemma 4.2. In particular, we will demonstrate in the experiment section that when the loss function is non-convex in parameters, the recovered parameter using MVI is closer to the ground truth than that using the SGD (see Table 1).

Moreover, we remark that the same order of convergence holds when F in (4) is estimated by the empirical average of *mini-batches* of training data. In particular, the proof of Theorem 4.3 only requires access to an unbiased estimator of F , so that the batch size can range from one to N , where N is the size of the training data.

Corollary 4.4 (Prediction error bound for test loss). *Fix an $\epsilon > 0$. For any test signal X_t , assume $N > C_t/\epsilon$. For a generic loss function $\mathcal{L} : (X, Y) \rightarrow \mathbb{R}_+$, which measures the error between $\mathbb{E}[Y|X]$ and Y , denote $\mathcal{L}^*(X_t, Y_t)$ (resp. $\hat{\mathcal{L}}(X_t, Y_t)$) as the loss under the true (resp. estimated) model. Then,*

1. When \mathcal{L} is the mean-square error (MSE) loss,

$$\mathbb{E}_{\bar{\Theta}_L^{(T)}} \{ |\hat{\mathcal{L}}(X_t, Y_t) - \mathcal{L}^*(X_t, Y_t)| \} \leq \epsilon.$$

2. When \mathcal{L} is the binary cross-entropy loss,

$$\mathbb{E}_{\bar{\Theta}_L^{(T)}} \{ |\hat{\mathcal{L}}(X_t, Y_t) - \mathcal{L}^*(X_t, Y_t)| \} \leq \sum_{i=1}^n Y_{t,i}^T \ln \left(\frac{E_{t,i}}{E_{t,i} - \epsilon} \right) + (1 - Y_{t,i}^T) \ln \left(\frac{1 - E_{t,i}}{1 - E_{t,i} - \epsilon} \right),$$

where $E_{t,i} := \mathbb{E}[Y_t|X_t]_i$ is the true conditional expectation of Y_t at node i , $\mathbf{1}$ and ϵ are vectors of 1 and ϵ , and the division is point-wise.

Remark 4.5 (When we can have $\kappa > 0$). Recall that $\kappa = \lambda_{\min}(\nabla \phi_L) \mathbb{E}_X[\lambda_{\min}(\eta^\top(X_L^*)\eta(X_L^*))]$. As we assumed the quantity $\mathbb{E}_X[\lambda_{\min}(\eta^\top(X_L^*)\eta(X_L^*))]$ is always lower bounded away from zero, we are only concern with the minimum eigenvalue of the gradient of ϕ acting on its inputs. Note that when ϕ_L is a point-wise function on its vector inputs, this gradient matrix is diagonal. In the case of the sigmoid function, we know that for any $y \in \mathbb{R}^n$

$$\lambda_{\min}[\nabla \phi_L]_y = \min_{i=1, \dots, n} \phi_L(y_i)(1 - \phi_L(y_i)),$$

which is bounded away from zero. In general, we only need that the point-wise activation is continuously differentiable with positive derivaties.

4.2 Case 2: modulus $\kappa = 0$

We may also encounter cases where the operator F is only monotone but not strongly monotone. For instance, let ϕ be the softmax function (applied row-wise to the filtered signal $\eta(X_L^*)\Theta_L \in \mathbb{R}^{n \times F}$), whose gradient matrix is thus block-diagonal. For any vector $z \in \mathbb{R}^F$, $\nabla \phi(z) = \text{diag}(\phi(z)) - \phi(z)\phi(z)^T$, which satisfies $\nabla \phi(z)\mathbf{1} = \mathbf{0}$ for any z (Gao & Pavel, 2018, Proposition 2). Therefore, the minimum eigenvalue of the gradient matrix of ϕ is always zero. Hence $\kappa = 0$.

In this case, note that the solution of $\text{VI}[F, \Theta]$ needs not be unique: a solution $\bar{\Theta}_L$ that satisfies the condition $\langle F(\bar{\Theta}_L), \Theta - \bar{\Theta}_L \rangle \geq 0, \forall \Theta \in \Theta$ may not be the true signal Θ_L^* . Nevertheless, suppose $F(\bar{\Theta}_L) = \mathbb{E}_{X,Y} \{ \eta(X_L^*)[\phi_L(\eta^\top(X_L^*))\bar{\Theta}_L] - Y \} = 0$. Because we assumed that the minimum singular value of $\eta(X_L^*)$

is always positive, we can still correctly predict the signal in expectation (a weaker guarantee than Theorem 4.2):

$$\mathbb{E}_X[\phi_L(\eta(X_L^*)\bar{\Theta}_L)] = \mathbb{E}_X[\phi_L(\eta(X_L^*)\Theta_L^*)].$$

Hence, we directly approximate the zero of F , by using the operator extrapolation method (OE) in (Kotsalis et al., 2020). We then have a similar ℓ_p performance guarantee in prediction:

Theorem 4.6 (Prediction error bound for model recovery, monotone F). *Suppose we run the OE algorithm (Kotsalis et al., 2020) for T iterations with $\lambda_t = 1$, $\gamma_t = [4K_2]^{-1}$, where K_2 is the Lipschitz constant of F . Let R be uniformly chosen from $\{2, 3, \dots, T\}$. Then for $p \in [2, \infty]$,*

$$\mathbb{E}_{\bar{\Theta}_L^{(R)}}\{\|\mathbb{E}_X\{\sigma_{\min}(\eta^\top(X_L^*))[\widehat{\mathbb{E}}[Y_t|X_t] - \mathbb{E}[Y_t|X_t]]\}\|_p\} \leq T^{-1/2}C_t'',$$

where $\sigma_{\min}(\cdot)$ denotes the minimum singular value of its input matrix and the constant $C_t'' := 3\sigma + 12K_2\sqrt{2\|\Theta_L^*\|_2^2 + 2\sigma^2/L^2}$, in which $\sigma^2 := \mathbb{E}[(F_i(\Theta_L) - F(\Theta_L))^2]$ is the variance of the unbiased estimator.

The convergence rate in Theorem 4.6 is also unaffected by the batch size, which only serves to reduce the variance. In addition, Theorem 4.6 requires R be uniformly chosen from $\{2, 3, \dots, T\}$, so that the theoretical guarantee holds at a random training epoch. In theory, this assumption is necessary to ensure a decrease of the norm of the monotone operator ((Kotsalis et al., 2020), Eq. (3.20)). In practice, we observed that the epoch that leads to the highest validation accuracy might not occur at the end of T training epochs, so this assumption is reasonable based on empirical evidence.

4.3 Equivalence between monotone operator and gradient of parameters

In practice, neural networks, including one-layer ones, are commonly trained via empirical loss minimization, in contrast to solving MVI. Nevertheless, we will show that under the cross-entropy loss, when ϕ is either the sigmoid function or the softmax function, the monotone operator F defined in (4) is exactly the expectation of the gradient of the loss with respect to parameters. As a result, both methods yield the same last-layer training dynamics, and previous guarantee also apply to gradient-based methods in such cases.

For notation simplicity, we consider a generic pair of input signal $X \in \mathbb{R}^C$ and categorical output $Y \in \{0, \dots, F\}^2$. Recall that X_L in (1) is the nonlinear feature transformation from the previous $L - 1$ layers. Given parameters $\Theta := \{\Theta_1, \dots, \Theta_L\}$ for L layers, we simplify the model $\mathbb{E}[Y|\eta_L(X_L), \Theta_L]$, which is based purely on the last layer parameter Θ_L as

$$\mathbb{E}[Y|\eta_L(X_L), \Theta_L] := \phi(\eta_L(X_L)\Theta_L), \tag{9}$$

²In GNN, $X \in \mathbb{R}^{n \times C}$ and $Y \in \{0, \dots, F\}^n$, but we can easily apply the same analyses at each node as the loss sums over nodes.

where $\mathbb{E}[Y|\eta_L(X_L), \Theta_L^*]$ is the true model. Now, the cross-entropy loss $\mathcal{L}(Y, \Theta_L)$ is

$$\mathcal{L}(Y, \Theta_L) := -Y \ln(\phi(\eta_L(X_L)\Theta_L)) - (1 - Y) \ln(1 - \phi(\eta_L(X_L)\Theta_L)) \quad Y \in \{0, 1\}. \quad (10)$$

$$\mathcal{L}(Y, \Theta_L) := -e_Y^T \ln(\phi(\eta_L(X_L)\Theta_L)) \quad Y \in \{0, \dots, F\}, F > 1. \quad (11)$$

In (10), $\phi(x) = \exp(x)/(1 + \exp x)$ is the sigmoid function applied point-wise. In (11), e_k is the k^{th} standard basis vector in \mathbb{R}^{F+1} and $\phi(\mathbf{x}) = \exp(\mathbf{x}_i)/\sum_j \exp(\mathbf{x}_j)$ is the softmax function applied row-wise. We now have the following proposition, whose proof can be found in Appendix A.

Proposition 4.7 (The equivalence between MVI and parameter gradient). *Consider a generic pair of input signal X and random realization Y following the model (9) under an arbitrary nonlinear transformation $\eta_L(X_L)$. If $Y \in \{0, 1\}$ as in binary (resp. $\{0, \dots, F\}$ as in multi-class for $F > 1$) classification, with ϕ being the sigmoid (resp. softmax) function under the cross-entropy loss $\mathcal{L}(Y, \Theta)$ defined in (10) (resp. (11)), we have that for any parameter Θ*

$$\mathbb{E}_{X,Y}[\nabla_{\Theta_L} \mathcal{L}(Y, \Theta_L)] = F(\Theta_L),$$

where the monotone operator $F(\Theta_L)$ substitutes $\eta_L(X_L)$ and Θ_L in (4).

4.4 Imprecise graph knowledge

Because graph knowledge is rarely perfectly known, the robustness of the algorithm with imprecise graph topology knowledge is important in practice for node classification. Thus, we want to analyze the difference in prediction quality when the true graph adjacency matrix W is estimated by another W' . For simplicity, we concentrate on the GCN case and drop certain super/sub-scripts (e.g., $X = X_L^*$ and $\Theta^* = \Theta_L^*$) and denote $\eta(X)$ under W (resp. W') as $L_g X$ (resp. $L'_g X$). Moreover, for a given $k \in \{1, \dots, n\}$, we can decompose L_g as $L_g = L_g^+ + L_g^-$, where $L_g^+ := U\Lambda^+U^T$, $\Lambda^+ = \text{diag}(\lambda_1, \dots, \lambda_k, \mathbf{0})$ denotes the high-energy portion of the filter (similarly for L_g^-).

We show that under certain assumptions on the similarity between high/low-portions of the true and estimated graph filters, there exists a solution $\Theta_{L'}^*$ that can lead to prediction error between $\mathbb{E}[Y|X]$ under Θ_L^* and $\Theta_{L'}^*$. In particular, $\Theta_{L'}^*$ is the solution of $\text{VI}[F, \Theta]$ if ϕ_L is the sigmoid function so that we can guarantee a small prediction error in expectation based on earlier results in such cases.

Proposition 4.8 (Quality of minimizer under model mismatch). *Fix an $\epsilon > 0$. Assume that (1) $L_g^+ = L'^+_g$ (2) $\|L'^-_g - L^-_g\|_2 \leq \epsilon/[K\mathbb{E}_X\|X^-\|]$, where K is the Lipschitz continuous constant for ϕ_L and X^- belongs to the span of L^-_g and L'^-_g . Then, there exists $\Theta_{L'}^*$ such that*

$$\|\mathbb{E}[Y|X] - \mathbb{E}[Y|X']\|_2 \leq \epsilon\|\Theta_{L'}^*\|_2,$$

where $\mathbb{E}[Y|X]'$ denotes the conditional expectation under L'_g and $\Theta_{L'}^*$.

5 Experiments

We test and compare SVI in Algorithm 1 with SGD on several experiments: one-layer model recovery and prediction, two-layer fully-connected (FC) network classification and, two/three-layer graph convolutional networks (GCN) model recovery on random graphs, and three-layer real-data network node classification. We aim to compare the performance of SVI and SGD. The code is available at <https://github.com/hamrel-cxu/SVI-NN-training>.

5.1 Result summary

We first provide a summary of the extensive experiments being performed.

One-layer networks (Sec. 5.3.1 and Appendix B.1): We had theoretical guarantees in Section 4. When data are generated from a non-convex probit model, SVI outperforms SGD with much smaller parameter recovery error and smaller/competitive training and/or test losses and/or errors (see Table 1). When SVI is identical to SGD (Proposition 4.7), we verify the insensitivity of SVI to batch size (see Figure 8), as remarked after Theorems 4.3 and 4.6.

Two-layer networks (Sec. 5.3.2 & 5.3.3 and Appendix B.2): Without acceleration techniques such as batch normalization (Ioffe & Szegedy, 2015b) (BN), SVI consistently reaches smaller training and/or test losses and/or errors than SGD throughout training epochs (see Sec. 5.3.2 & 5.3.3). When BN is used, SGD in some cases eventually reaches smaller errors or losses than SVI. However, SVI almost always reaches very small errors or losses with a few training epochs, and it takes SGD a lot more epochs to reach the same values (see Appendix B.2).

Three-layer networks (Sec. 5.4 and Appendix B.3 & B.4: On real test data, SVI without BN acceleration almost always reaches smaller classification error and higher weighted F_1 scores than SGD, with faster initial convergence as well (see Sec. 5.4). Meanwhile, BN worsens SVI and improves SGD, but SVI maintains fast initial convergence, and SVI without BN is still competitive or better than SGD with BN (see Appendix B.3). On simulated data, SGD with BN almost always eventually reaches smaller errors and losses than SVI with BN, but SVI still enjoys fast initial convergence, and the smallest eventual error and loss by SVI without BN is smaller than most eventual errors and losses by SGD with BN (see Appendix B.4).

Beyond three-layers networks (Sec. 5.4 and Appendix B.5): We compare and contrast SVI trained under SGD or Adam with SGD or Adam on one of the large-scale realistic node classification dataset from the Open Graph Benchmark (Hu et al., 2020). In particular, the results show that under different choices of the number of hidden nodes, SVI under either SGD or Adam yields improved efficiency during the initial stages of training and reaches competitive overall training performances.

5.2 Setup and Comparison Metrics

Setup. All implementation are done using `PyTorch` (Paszke et al., 2019) and `PyTorch Geometric` (Fey & Lenssen, 2019) (for GNN). To ensure fair comparison, we carefully describe the experiment setup. In particular, the following inputs are *identical* to both `SVI` and `SGD` in each experiment.

- Data: (a) the size of training and test data (b) batch (batch size and samples in mini-batches).
- Model: (a) architecture (e.g., layer choice, activation function, hidden neurons) (b) loss function.
- Training regime: (a) parameter initialization (b) hyperparameters for backpropagation (e.g., learning rate, momentum factor, acceleration) (c) total number of epochs (d) acceleration techniques (e.g., BN).

In short, all except the way gradients are defined are kept the same for each comparison—our proposed `SVI` backpropagates gradients with respect to hidden input and transform the gradient back to parameter domain, whereas `SGD` do so with respect to parameters in each hidden layer.

Comparison metrics. For a random feature $X \in \mathbb{R}^{n \times C}$, where n is the number of graph nodes and C is the input dimension, let the true (or predicted) model be $\mathbb{E}[Y|X, \Theta] \in \mathbb{R}^{n \times F}$ (or $\mathbb{E}[Y|X, \hat{\Theta}]$), where F is the output dimension. Given N realized pairs $\{(X_i, Y_i)\}_{i=1}^N$ where N denotes either the training or test sample size, we employ the following metrics for various tasks.³

$$\text{MSE loss} := N^{-1} \sum_{i=1}^N \sum_{j=1}^n \|\mathbb{E}[Y_i|X_i, \hat{\Theta}]_j - Y_{i,j}\|_2 \quad (12)$$

$$\text{Cross-entropy loss} := N^{-1} \sum_{i=1}^N \sum_{j=1}^n Y_{i,j}^T \mathbb{E}[Y_i|X_i, \hat{\Theta}]_j \quad (13)$$

$$\text{Classification error} := (n \cdot N)^{-1} \sum_{i=1}^N \sum_{j=1}^n \sum_{f=1}^F \mathbf{1}(Y_{i,j,f} \neq \hat{Y}_{i,j,f}) \quad (14)$$

$$\ell_p \text{ parameter recovery error} := \|\hat{\Theta} - \Theta\|_p \quad (15)$$

$$\ell_p \text{ model recovery error} := N^{-1} \sum_{i=1}^N \sum_{j=1}^n \|\mathbb{E}[Y_i|X_i, \hat{\Theta}]_j - \mathbb{E}[Y_i|X_i, \Theta]_j\|_p. \quad (16)$$

For GCN model recovery We let $p = 2$ or ∞ in (15) and (16) and when $p = 2$, compute the relative error using $\|\Theta\|_p$ or $N^{-1} \sum_{i=1}^N \sum_{j=1}^n \|\mathbb{E}[Y_i|X_i, \Theta]_j\|_p$ on the denominator. In addition, all results are averaged over three random trials, in which features X_i are redrawn for simulated example and networks re-initialized. We show standard errors in tables as brackets and in plots as error bars. Partial results are shown due to space limitation, where Appendix B contains the extensive results.

5.3 Synthetic Data Experiments

Notation-wise, $X \sim \mathcal{N}(a, b)$ means the random variable X follows a normal distribution with mean a and variance b^2 ; N (resp. N_1) denotes the size of training (resp. test) sample, lr denotes the learning rate, B denotes the batch size, and E denotes training epochs.

³We one-hot encode Y_i in multi-class classification to make sure certain operations are well-defined.

Probit model Feature dimension	ℓ_2 para recovery error		MSE loss				Classification error			
	SGD	SVI	SGD train	SVI train	SGD test	SVI test	SGD train	SVI train	SGD test	SVI test
50	0.596 (5.9e-05)	0.485 (1.1e-04)	0.039 (4.1e-04)	0.034 (4.0e-04)	0.043 (1.8e-04)	0.038 (2.3e-04)	0.034 (7.1e-04)	0.035 (8.9e-04)	0.046 (9.4e-04)	0.049 (1.4e-03)
100	0.683 (5.2e-05)	0.593 (8.4e-05)	0.032 (6.1e-05)	0.026 (5.5e-05)	0.043 (6.6e-04)	0.039 (7.0e-04)	0.021 (5.4e-04)	0.021 (1.4e-04)	0.053 (2.4e-03)	0.054 (9.4e-04)
200	0.78 (2.1e-04)	0.717 (2.3e-04)	0.025 (3.8e-05)	0.019 (1.0e-05)	0.045 (1.2e-03)	0.041 (1.0e-03)	0.011 (7.6e-04)	0.011 (8.3e-04)	0.058 (3.3e-03)	0.055 (3.6e-03)

Table 1: Non-convex one-layer probit model, with identical learning rate for both. We show average results at end of 200 epochs, with standard errors in brackets. SVI consistently reaches smaller parameter recovery error and MSE loss than SGD, and SGD may be slightly better in terms of classification error. Metrics are defined in (15), (12), and (14), respectively.

Two-moon data # Hidden neurons	MSE loss				Classification error			
	SGD train	SVI train	SGD test	SVI test	SGD train	SVI train	SGD test	SVI test
8	0.00062 (4.0e-05)	0.00054 (2.1e-05)	0.06709 (4.8e-03)	0.05993 (4.5e-03)	0.08333 (7.2e-03)	0.076 (3.8e-03)	0.098 (6.6e-03)	0.08933 (1.1e-02)
16	0.00053 (7.7e-05)	0.00042 (8.5e-05)	0.05852 (7.1e-03)	0.04702 (7.7e-03)	0.06533 (1.5e-02)	0.052 (1.3e-02)	0.078 (9.6e-03)	0.06333 (1.3e-02)
32	0.00022 (2.9e-05)	0.00014 (1.8e-05)	0.02375 (2.2e-03)	0.01517 (6.9e-04)	0.01867 (3.8e-03)	0.01533 (2.4e-03)	0.01733 (2.2e-03)	0.016 (9.4e-04)
64	0.00016 (1.7e-05)	8e-05 (1.4e-05)	0.01774 (1.2e-03)	0.00872 (1.0e-03)	0.01 (2.5e-03)	0.006 (1.6e-03)	0.01067 (3.0e-03)	0.00933 (2.0e-03)

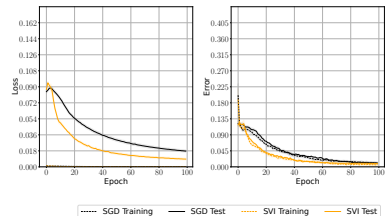


Table 2: Two-moon data, binary classification, with identical learning rate and ReLU activation for both. We show average results at end of epochs, with standard errors in brackets. SVI consistently reaches smaller training and/or test MSE loss and/or classification errors than SGD across different number of hidden neurons.

Figure 1: Two-moon data, 64 hidden neurons, with MSE loss (left) and classification error (right). SVI shows faster convergence.

5.3.1 One-layer model recovery and prediction. We start with model recovery and prediction on data generated from a one-layer probit model, which leads to non-convex objectives. Specifically, for each $i \geq 1$, $y_i \in \{0, 1\}$ and $\mathbb{E}[y_i | X_i] = \Phi(X_i^T \beta + b)$, where $X_i \in \mathbb{R}^p$, $X_{ij} \stackrel{i.i.d.}{\sim} \mathcal{N}(0.05, 1)$, $\beta_j \stackrel{i.i.d.}{\sim} \mathcal{N}(-0.05, 1)$, and $b \sim \mathcal{N}(-0.1, 1)$. Here, $\Phi(z) = \mathbb{P}(Z \leq z)$, $Z \sim \mathcal{N}(0, 1)$. We let $N = 2000$, $N_1 = 500$, and use a fully-connected one-layer network. The goal is to recover parameter $\{\beta, b\}$ via minimizing the non-convex MSE objective (i.e., $N^{-1} \sum_{i=1}^N \|y_i - \Phi(X_i^T \beta + b)\|_2$) and make prediction on test samples. We let $B = 200$ and $E = 200$ and use $\text{lr}=0.005$ and $\text{momentum} = 0.9$.

Table 1 shows that SVI consistently reaches small parameter recovery error than SGD across feature dimensions, with 8~10% difference. Moreover, the same phenomenon appears in both training and test MSE losses. Lastly, SGD may reach a smaller classification error, but the difference is very small. See Appendix B.1, Figure 7 for additional results that illustrates model intermediate convergence results.

We also examine the insensitivity of SVI to changes in batch size when data are generated from a one-layer GCN model with sigmoid activation. We note that when the input feature dimension C is fixed, SVI nearly converges to the same MSE loss defined in (12) and the same ℓ_∞ error defined in (16), regardless of the batch size B ; the differences are only caused by the fewer number of iterations when B increases. The setup is described in Appendix B.1 and detailed results are in Figure 8.

5.3.2 Two-layer FC network classification. We next consider the classification problem of determining the cluster label of each sample of a simulated two-moon dataset. Figure 9a visualizes the dataset. We use a two-layer fully-connected network with ReLU (layer 1) and softmax (layer 2) activation. We let

Large Graph # Hidden neurons	ℓ_2 model recovery test error				MSE test loss				ℓ_∞ model recovery test error			
	SGD (Known)	SGD (Perturbed)	SVI (Known)	SVI (Perturbed)	SGD (Known)	SGD (Perturbed)	SVI (Known)	SVI (Perturbed)	SGD (Known)	SGD (Perturbed)	SVI (Known)	SVI (Perturbed)
2	0.116 (3.4e-03)	0.117 (3.6e-03)	0.091 (8.4e-03)	0.092 (7.5e-03)	0.25 (1.9e-04)	0.25 (2.0e-04)	0.249 (4.2e-04)	0.249 (3.6e-04)	0.129 (4.3e-03)	0.13 (4.5e-03)	0.1 (8.6e-03)	0.102 (7.3e-03)
4	0.1 (8.1e-03)	0.101 (7.6e-03)	0.078 (6.2e-03)	0.081 (5.6e-03)	0.25 (4.0e-04)	0.25 (3.7e-04)	0.248 (3.0e-04)	0.249 (2.8e-04)	0.109 (8.4e-03)	0.11 (7.8e-03)	0.087 (4.8e-03)	0.091 (3.8e-03)
8	0.084 (7.7e-03)	0.086 (7.0e-03)	0.067 (5.5e-04)	0.07 (4.4e-04)	0.249 (3.4e-04)	0.249 (3.2e-04)	0.248 (4.0e-06)	0.248 (1.0e-06)	0.088 (7.2e-03)	0.091 (6.5e-03)	0.076 (8.2e-04)	0.083 (5.2e-04)
16	0.08 (7.3e-03)	0.081 (6.5e-03)	0.066 (3.3e-04)	0.07 (2.1e-04)	0.249 (2.8e-04)	0.249 (2.5e-04)	0.248 (6.0e-06)	0.248 (1.0e-05)	0.087 (7.8e-03)	0.089 (6.6e-03)	0.075 (4.6e-04)	0.082 (1.4e-04)
32	0.082 (8.1e-03)	0.084 (7.5e-03)	0.066 (5.6e-05)	0.07 (6.2e-05)	0.249 (3.6e-04)	0.249 (3.4e-04)	0.248 (1.1e-05)	0.248 (1.2e-05)	0.089 (8.8e-03)	0.091 (7.9e-03)	0.075 (1.7e-04)	0.082 (1.0e-04)

Table 3: Two-layer GCN model recovery on the large random graph, with identical learning rate and ReLU activation for both SVI and SGD under $B = 100$. The true data are generated from a two-layer GCN. We observe consistently better model recovery performance by SVI, regardless of the number of hidden neurons for estimation, comparison metrics, and whether graph is perturbed. Metrics are defined in (16) and (12) respectively.

$N = N_1 = 500$, $\text{lr}=0.15$, $B = 100$, and $E = 100$. No batch normalization is used.

Table 2 shows that SVI consistently reaches smaller MSE losses and classification errors on training and test data across different number of hidden neurons. Figure 1 shows that SVI also converges faster than SGD throughout epochs. See Appendix B.2, Figure 9 for additional results that illustrates model intermediate convergence results.

5.3.3 Two-layer GCN model recovery. Given a graph $G = (\mathcal{V}, \mathcal{E})$, $|\mathcal{V}| = n$ and a signal $X_i \in \mathbb{R}^{n \times C}$, we generate $Y_i \in \mathbb{R}^{n \times F}$, where $\mathbb{E}[Y_i|X_i]$ is a two/three-layer GCN model with ReLU (layer 1/layer 1 and 2) and sigmoid (layer 2/layer 3) activation. We let $C = 2$ and $F = 1$ and let the true number of hidden nodes in each hidden layer always be 2. Entries of all true weight and bias parameters (resp. features X_i) are i.i.d. samples from $N(1, 1)$ (resp. $N(0, 1)$) under a fixed seed (resp. fixed seeds per random trial). We consider both small ($n = 15$) and large ($n = 40$) graphs, where $\mathbb{P}[(i, j) \in \mathcal{E}] = 0.15$; Figure 10 visualizes the graphs. The true parameters are identical in both graphs. Meanwhile, we examine the recovery performance either when the true graph (i.e., \mathcal{E}) is known or when the edge set are perturbed—a p fraction of edges in \mathcal{E} and in \mathcal{E}^C are randomly discarded and inserted, where \mathcal{E}^C denotes edges in a fully-connected graph that does not exist in \mathcal{E} . We set $p = 0.2$ (resp. 0.05) for small (resp. large) graphs. Finally, we let $N = 2000$, $N_1 = 2000$, and $E = 200$. We use $\text{lr}=0.001$, momentum = 0.99, and also the Nesterov momentum (Sutskever et al., 2013).

Table 3 shows that without BN for both methods, SVI consistently reaches smaller ℓ_2 model recovery error for the two-layer GCN, even in an over-parametrized network (e.g., use 32 hidden neurons in estimation when the ground truth has only two neurons). The pattern is consistent even if the graph information is perturbed. The exact pattern persists when we measure the model recovery in terms of relative error in MSE loss or ℓ_∞ model recovery error. Figure 2 (large graph) also shows that SVI consistently converges faster than SGD.

In Appendix B.2, we present additional results regarding model recovery on the small random graph (see Table 6), intermediate convergence results (see Figure 12), and sensitivity of SVI and SGD to changes in batches sizes, without and with BN (see Tables 7 and 8 for results at the final epochs and Figure 13 and 14 for intermediate convergence results). Overall, SVI converges faster even if SGD uses the BN acceleration

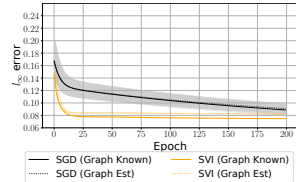


Figure 2: ℓ_∞ model recovery error on the large random graph. SVI consistently reaches smaller error under faster convergence, even just after the first training epoch.

California solar data	MSE loss				Classification error				Weighted F_1 score			
	# Hidden neurons	SGD Training	SGD Test	SVI Training	SVI Test	SGD Training	SGD Test	SVI Training	SVI Test	SGD Training	SGD Test	SVI Training
8	0.217 (6.6e-03)	0.219 (5.9e-03)	0.195 (7.0e-03)	0.207 (5.7e-03)	0.297 (8.1e-03)	0.321 (4.5e-03)	0.296 (1.4e-02)	0.318 (1.5e-02)	0.706 (8.1e-03)	0.675 (5.6e-03)	0.703 (1.5e-02)	0.681 (1.5e-02)
16	0.229 (7.6e-03)	0.225 (7.3e-03)	0.194 (7.3e-03)	0.204 (6.4e-03)	0.314 (1.3e-02)	0.335 (6.8e-03)	0.292 (1.7e-02)	0.305 (1.7e-02)	0.687 (1.3e-02)	0.655 (9.4e-03)	0.709 (1.7e-02)	0.695 (1.7e-02)
32	0.224 (2.7e-03)	0.223 (1.4e-03)	0.185 (2.5e-03)	0.196 (2.3e-03)	0.297 (3.4e-03)	0.333 (7.4e-03)	0.274 (4.4e-03)	0.292 (5.0e-03)	0.704 (3.8e-03)	0.659 (8.4e-03)	0.727 (4.0e-03)	0.708 (5.1e-03)
64	0.213 (4.5e-04)	0.211 (9.6e-04)	0.18 (5.1e-04)	0.189 (3.9e-04)	0.283 (2.5e-03)	0.308 (6.0e-03)	0.262 (2.1e-03)	0.27 (1.5e-03)	0.719 (2.6e-03)	0.689 (6.7e-03)	0.738 (1.7e-03)	0.73 (1.4e-03)

Table 4: California solar binary ramping event detection under a three-layer GCN model, with identical learning rate and ReLU activation for both. In addition to MSE loss and classification loss, we also use the weighted F_1 score as an additional metric, which weighs F_1 score in each class by its support. SVI consistently outperforms SGD on all these metrics on both training and test data.

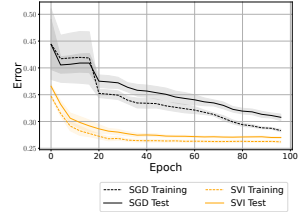


Figure 4: Classification error under 64 neurons in both hidden layers. SVI converges faster than SGD on both training and test data, especially in the initial stage.

and SVI can yield better/competitive eventual results.

To better understand how SVI update parameters, Figure 3 zooms in the dynamics for 16 neurons (right figure) and shows the corresponding ℓ_∞ model recovery test error (left figure). Regarding the right figure, we plot the norm of first-layer neuron weights, where the norm is defined in terms of the inner product with initial weights, against the second-layer neuron weights, which are scalars because $F = 1$. One circle represents one neuron, with arrows representing the direction of moving along the initial weights. We then connect the initial and final dots to indicate the displacement of neurons. The same visualization techniques are used in (Pellegrini & Biroli, 2020). It is clear that SVI displaces neurons further after 200 epochs, which is anticipated in Remark 3.1. In this case, we think it can be beneficial due to the much faster error convergence.

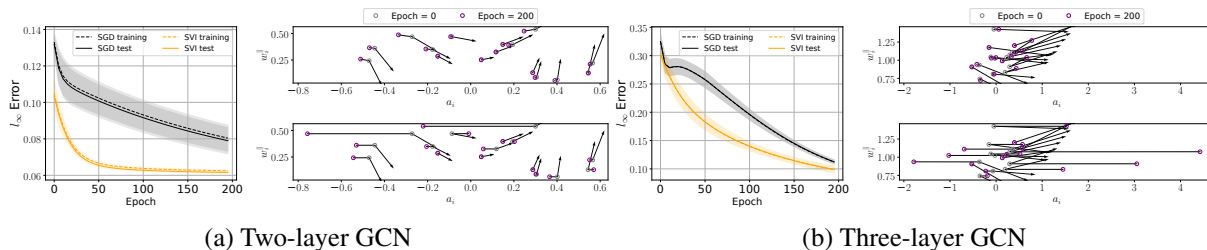


Figure 3: ℓ_∞ model recovery error on the small graph with 16 neurons under $B = 100$, with identical learning rate and Softplus activation for both. Left: relative ℓ_∞ error in training and test data, assuming the true graph is known. Right: visualization of the training dynamics. After 200 epochs, SVI displaces the neurons from their initial position further than SGD, where such displacement also leads to much faster convergence in the relative error.

5.4 Real-data Network Prediction

We lastly use three-layer GCN for real-data experiments, where both layers share the same number of hidden neurons with the ReLU activation. The output layer uses sigmoid (binary node classification) or softmax (multi-class node classification). We fix $\text{lr} = 0.001$, momentum = 0.99, and use the Nesterov momentum (Sutskever et al., 2013).

Traffic data	Cross-Entropy loss				Classification error				Weighted F_1 score			
	SGD Training	SGD Test	SVI Training	SVI Test	SGD Training	SGD Test	SVI Training	SVI Test	SGD Training	SGD Test	SVI Training	SVI Test
8	0.837 (7.0e-03)	0.834 (1.1e-02)	0.967 (6.2e-03)	0.969 (5.5e-03)	0.397 (1.3e-02)	0.414 (1.5e-02)	0.412 (1.6e-02)	0.427 (1.6e-02)	0.572 (2.9e-02)	0.554 (2.9e-02)	0.572 (2.4e-02)	0.558 (2.3e-02)
16	0.808 (5.6e-03)	0.804 (4.1e-03)	0.955 (3.3e-03)	0.956 (4.0e-03)	0.391 (1.3e-02)	0.411 (1.2e-02)	0.37 (3.8e-03)	0.384 (7.0e-03)	0.576 (3.1e-02)	0.556 (3.0e-02)	0.624 (7.3e-03)	0.61 (1.0e-02)
32	0.791 (5.7e-03)	0.787 (6.5e-03)	0.939 (3.4e-03)	0.941 (3.6e-03)	0.366 (5.9e-03)	0.383 (7.9e-03)	0.358 (4.5e-03)	0.37 (4.9e-03)	0.628 (6.7e-03)	0.611 (9.0e-03)	0.641 (4.6e-03)	0.629 (5.0e-03)
64	0.791 (2.0e-03)	0.787 (2.2e-03)	0.933 (2.1e-03)	0.935 (2.1e-03)	0.36 (2.7e-03)	0.375 (4.4e-03)	0.346 (1.7e-03)	0.358 (1.6e-03)	0.637 (2.8e-03)	0.622 (4.7e-03)	0.652 (2.0e-03)	0.641 (1.8e-03)

Table 5: Traffic data multi-class anomaly detection under a three-layer GCN model, with identical learning rate and ReLU activation for both. We note that SVI remains competitive or outperforms SGD in terms of classification error and weighted F_1 scores, with clear improvement when hidden neurons increase. However, SVI reaches much larger cross-entropy losses, which we think are benign (see Section 5.4.2 for justification).

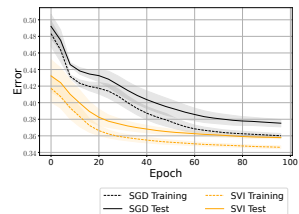


Figure 5: Classification error under 64 neurons in both hidden layers. SVI converges faster, especially after a single training epoch.

5.4.1 Binary solar ramping prediction. The raw solar radiation data are retrieved from the National Solar Radiation Database for 2017 and 2018. We consider data from 10 cities downtown in California and from 9 locations in downtown Los Angeles, where each city or location is a node in the network. The goal is to identify ramping events daily, abrupt changes in the solar power generation. Thus, $Y_{t,i} = 1$ if node i at day t experiences a ramping event. We define feature $X_t := \{Y_{t-1}, \dots, Y_{t-d}\}$ as the collection of past d days of observation and pick $d = 5$. We estimate edges via a k -nearest neighbor approach based on the correlation between training ramping labels, with $k = 4$. Data in 2017 are used for training ($N = 360$) and the rest for testing ($N_1 = 365$), and we let $B = 30$ and $E = 100$.

Table 4 shows that SVI almost always outperforms SGD under any metric on both training and test data. The pattern is consistent across different numbers of hidden neurons. Figure 4 also shows that SVI converges faster than SGD, which aligns with earlier simulation results. See Appendix B.3, Figure 15 (CA) and 16 (LA) for intermediate convergence results, including those under BN.

5.4.2 Multi-class traffic flow anomaly detection. The raw bi-hourly traffic flow data are from the California Department of Transportation, where we collected data from 20 non-uniformly spaced traffic sensors in 2020. Data are available hourly, with $Y_{t,i} = 1$ (resp. 2) if the current traffic flow lies outside the upper (resp. lower) 90% quantile over the past four days of traffic flow of its nearest four neighbors based on sensor proximity. As before, we define feature X_t as the collection of past d days of observation and set $d = 4$, where the edges include the nearest five neighbors based on location. Data in the first nine months are training data (e.g., $N = 6138$) and the rest for testing ($N_1 = 2617$). We let $B = 600$ and $E = 100$ and use the cross-entropy loss to test the performance of SVI under alternative loss functions.

Table 5 shows that SVI reaches smaller training and test classification error for large hidden neurons and remains competitive when fewer neurons are used. In terms of weighted F_1 scores, SVI also reaches higher training and test scores in all except one choice of hidden neurons. Lastly, we note that SVI results in much larger cross-entropy losses, which might happen if the predicted posterior probabilities by SVI are more uniform than SGD. In this case, such behavior is benign due to smaller test errors of SVI, which likely happen because there is potential ambiguity in the test data: the true posterior probabilities in certain portions do not concentrate on a specific class. As a result, more uniform posterior probability predictions by

SVI better estimate the true probabilities, leading to smaller test errors and higher weighted F_1 scores. See Appendix B.3, Figure 17 for intermediate convergence results.

5.4.3 Multi-class large-scale OGB node classification. We lastly demonstrate the applicability of SVI on the large `ogbn-arxiv` graph provided by the Open Graph Benchmark (Hu et al., 2020, 2021). The graph is much larger than earlier examples, and we also use wider and deeper models—the graph nodes are papers to be classified into categories and edges denote citation among papers; it has ~ 170 thousand nodes, 1.16 million edges, 128-dimensional node features, and 40 node classes. This graph is significantly larger than earlier examples. We train four-layer GCN models with hidden nodes kept at 512, which are both wider and deeper than earlier models. We optimize with SVI, SVI-Adam, SGD, and Adam, and train for a fixed $E = 500$ epochs. We also use batch normalization and dropouts in the architecture. Figure 6 shows that SVI or SVI-Adam yield comparable results to SGD or Adam. In addition, the bottom row shows clearly that SVI and SVI-Adam converge much faster than SGD and Adam during initial epochs, where such behavior also appears in earlier experiments. We believe this faster initial convergence is particularly useful on large-scale experiments, where it is computationally demanding to run many training epochs. See Appendix B.5 for results under different number of hidden neurons.

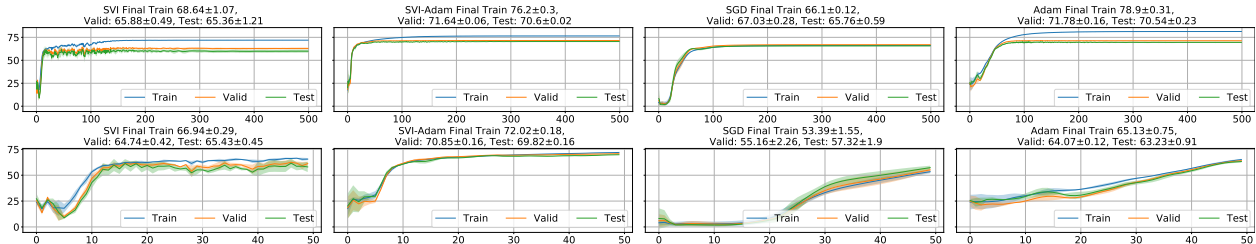


Figure 6: Classification accuracies (train/validation/test) on the large-scale `ogbn-arxiv` dataset from the Open Graph Benchmark. The top (resp. bottom) row shows accuracies over all (resp. initial 50) training epochs, where the term “final” indicates results at the highest validation accuracy. SVI or SVI-Adam still improves initial convergence with competitive final accuracies than SGD or Adam.

6 Conclusion

We have presented a new monotone operator variational inequality (VI) approach for training neural networks, particularly training graph neural networks, which enjoys strong prediction guarantees in training one-layer neural networks. In training general multi-layer neural networks, the proposed method can obtain faster convergence and make more accurate predictions relative to a comparable stochastic gradient descent algorithm, using extensive simulation and real-data study regarding various performance metrics.

At present, the following tasks remain open. Theoretically, the guarantees hold only when all except the last layers of the network are known. Instead, it is important to relax and quantify the level of knowledge we need for these layers to better explain the previous-layer heuristics of SVI. Methodologically, moving beyond decoupled features $\eta_l(X_l)$ and Θ_l as in (6) is important. Application-wise, it is useful to address a wider range of problems in GNN, including edge and graph classification (Zhou et al., 2020). We will explore them in the future.

Acknowledgement

The authors are partially supported by NSF DMS-2134037.

References

- Allen-Zhu, Z., Li, Y., and Song, Z. A convergence theory for deep learning via over-parameterization. In *International Conference on Machine Learning*, pp. 242–252. PMLR, 2019.
- Arora, S., Du, S. S., Hu, W., Li, Z., Salakhutdinov, R. R., and Wang, R. On exact computation with an infinitely wide neural net. In *Advances in Neural Information Processing Systems*, pp. 8139–8148, 2019a.
- Arora, S., Du, S. S., Hu, W., Li, Z., and Wang, R. Fine-grained analysis of optimization and generalization for overparameterized two-layer neural networks. *arXiv preprint arXiv:1901.08584*, 2019b.
- Defferrard, M., Bresson, X., and Vandergheynst, P. Convolutional neural networks on graphs with fast localized spectral filtering. *Advances in neural information processing systems*, 29:3844–3852, 2016.
- Du, S., Lee, J., Li, H., Wang, L., and Zhai, X. Gradient descent finds global minima of deep neural networks. In *International Conference on Machine Learning*, pp. 1675–1685. PMLR, 2019.
- Duchi, J. C., Hazan, E., and Singer, Y. Adaptive subgradient methods for online learning and stochastic optimization. In *J. Mach. Learn. Res.*, 2010.
- Facchinei, F. and Pang, J. S. Finite-dimensional variational inequalities and complementarity problems. 2003.
- Fey, M. and Lenssen, J. E. Fast graph representation learning with PyTorch Geometric. In *ICLR Workshop on Representation Learning on Graphs and Manifolds*, 2019.
- Gao, B. and Pavel, L. On the properties of the softmax function with application in game theory and reinforcement learning, 2018.
- Hamilton, W. L., Ying, R., and Leskovec, J. Inductive representation learning on large graphs. In *Proceedings of the 31st International Conference on Neural Information Processing Systems*, pp. 1025–1035, 2017.
- Hu, W., Fey, M., Zitnik, M., Dong, Y., Ren, H., Liu, B., Catasta, M., and Leskovec, J. Open graph benchmark: Datasets for machine learning on graphs. *arXiv preprint arXiv:2005.00687*, 2020.
- Hu, W., Fey, M., Ren, H., Nakata, M., Dong, Y., and Leskovec, J. Ogb-lsc: A large-scale challenge for machine learning on graphs. *arXiv preprint arXiv:2103.09430*, 2021.
- Ioffe, S. and Szegedy, C. Batch normalization: Accelerating deep network training by reducing internal covariate shift. *ArXiv*, abs/1502.03167, 2015a.

- Ioffe, S. and Szegedy, C. Batch normalization: Accelerating deep network training by reducing internal covariate shift. In Bach, F. and Blei, D. (eds.), *Proceedings of the 32nd International Conference on Machine Learning*, volume 37 of *Proceedings of Machine Learning Research*, pp. 448–456, Lille, France, 07–09 Jul 2015b. PMLR.
- Juditsky, A. and Nemirovski, A. On well-structured convex-concave saddle point problems and variational inequalities with monotone operators. *arXiv preprint arXiv:2102.01002*, 2021.
- Juditsky, A. B. and Nemirovsky, A. S. Signal recovery by stochastic optimization. *Autom. Remote. Control.*, 80:1878–1893, 2019.
- Kinderlehrer, D. and Stampacchia, G. An introduction to variational inequalities and their applications. 1980.
- Kingma, D. P. and Ba, J. Adam: A method for stochastic optimization. *CoRR*, abs/1412.6980, 2015.
- Kipf, T. N. and Welling, M. Semi-supervised classification with graph convolutional networks. In *5th International Conference on Learning Representations, ICLR 2017, Toulon, France, April 24-26, 2017, Conference Track Proceedings*. OpenReview.net, 2017.
- Kotsalis, G., Lan, G., and Li, T. Simple and optimal methods for stochastic variational inequalities, i: operator extrapolation. *arXiv preprint arXiv:2011.02987*, 2020.
- Lin, Q., Liu, M., Rafique, H., and Yang, T. Solving weakly-convex-weakly-concave saddle-point problems as weakly-monotone variational inequality. 2018.
- Mei, S., Montanari, A., and Nguyen, P.-M. A mean field view of the landscape of two-layer neural networks. *Proceedings of the National Academy of Sciences*, 115(33):E7665–E7671, 2018.
- Neyshabur, B., Tomioka, R., and Srebro, N. In search of the real inductive bias: On the role of implicit regularization in deep learning. *arXiv preprint arXiv:1412.6614*, 2014.
- Outrata, J., Kocvara, M., and Zowe, J. *Nonsmooth approach to optimization problems with equilibrium constraints: theory, applications and numerical results*, volume 28. Springer Science & Business Media, 2013.
- Paszke, A., Gross, S., Massa, F., Lerer, A., Bradbury, J., Chanan, G., Killeen, T., Lin, Z., Gimelshein, N., Antiga, L., Desmaison, A., Kopf, A., Yang, E., DeVito, Z., Raison, M., Tejani, A., Chilamkurthy, S., Steiner, B., Fang, L., Bai, J., and Chintala, S. Pytorch: An imperative style, high-performance deep learning library. In Wallach, H., Larochelle, H., Beygelzimer, A., d'Alché-Buc, F., Fox, E., and Garnett, R. (eds.), *Advances in Neural Information Processing Systems 32*, pp. 8024–8035. Curran Associates, Inc., 2019.
- Pellegrini, F. and Biroli, G. An analytic theory of shallow networks dynamics for hinge loss classification. *arXiv preprint arXiv:2006.11209*, 2020.

Pilanci, M. and Ergen, T. Neural networks are convex regularizers: Exact polynomial-time convex optimization formulations for two-layer networks. In *ICML*, 2020.

Sutskever, I., Martens, J., Dahl, G., and Hinton, G. On the importance of initialization and momentum in deep learning. In Dasgupta, S. and McAllester, D. (eds.), *Proceedings of the 30th International Conference on Machine Learning*, volume 28 of *Proceedings of Machine Learning Research*, pp. 1139–1147, Atlanta, Georgia, USA, 17–19 Jun 2013. PMLR.

Wu, Z., Pan, S., Chen, F., Long, G., Zhang, C., and Yu, P. S. A comprehensive survey on graph neural networks. *IEEE Transactions on Neural Networks and Learning Systems*, 32:4–24, 2019.

Zhou, J., Cui, G., Zhang, Z., Yang, C., Liu, Z., and Sun, M. Graph neural networks: A review of methods and applications. *ArXiv*, abs/1812.08434, 2020.

A Proofs

Proof of Lemma 4.1. We first verify the monotonicity of F by considering vectorized parameters, where for a matrix $A \in \mathbb{R}^{m \times n}$, $\text{vec}(A) \in \mathbb{R}^{mn}$ by stacking vertically columns of A . Note that this vectorization is simply used to make sure the Euclidean inner product between F and Θ_L is well-defined; the fundamental meaning of Θ_L (e.g., as the channel-mixing coefficient) remains unchanged. With an abuse of notation, we use the same Θ_L and Θ to denote the vectorized parameter and the corresponding parameter space. For any $\Theta_{1,L}, \Theta_{2,L} \in \Theta$,

$$\begin{aligned}
& \langle F(\Theta_{1,L}) - F(\Theta_{2,L}), \Theta_{1,L} - \Theta_{2,L} \rangle \\
&= \langle \mathbb{E}_X \{ \eta^\top(X_L^*) (\phi_L(\eta(X_L^*)\Theta_{1,L}) - \phi_L(\eta(X_L^*)\Theta_{2,L})) \}, \Theta_{1,L} - \Theta_{2,L} \rangle \\
&= \mathbb{E}_X \{ (\phi_L(\eta(X_L^*)\Theta_{1,L}) - \phi_L(\eta(X_L^*)\Theta_{2,L}))^\top (\eta(X_L^*)\Theta_{1,L} - \eta(X_L^*)\Theta_{2,L}) \} \\
&\geq \lambda_{\min}(\nabla \phi_L) \mathbb{E}_X \{ \|\eta(X_L^*)\Theta_{1,L} - \eta(X_L^*)\Theta_{2,L}\|_2^2 \} \quad (\text{If } \nabla \phi_L \text{ exists.}) \\
&\geq \underbrace{\lambda_{\min}(\nabla \phi_L) \mathbb{E}_X \{ \lambda_{\min}(\eta^\top(X_L^*)\eta(X_L^*)) \}}_{\kappa:=} \|\Theta_{1,L} - \Theta_{2,L}\|_2^2,
\end{aligned}$$

where κ is defined in (3). The first equality uses the fact that the Y part is cancelled and the first inequality holds when ϕ_L is *continuously differentiable* on its domain. If ϕ_L is only monotone on its domain, the the first inequality will only be greater than 0.

We then verify the K_2 -Lipschitz continuity of F . For any $\Theta_{1,L}, \Theta_{2,L} \in \Theta$,

$$\begin{aligned}
\|F(\Theta_{1,L}) - F(\Theta_{2,L})\|_2 &= \mathbb{E}_X \{ \|\eta^\top(X_L^*) (\phi_L(\eta(X_L^*)\Theta_{1,L}) - \phi_L(\eta(X_L^*)\Theta_{2,L}))\|_2 \} \\
&\leq \mathbb{E}_X \{ \|\eta^\top(X_L^*)\|_2 \|\phi_L(\eta(X_L^*)\Theta_{1,L}) - \phi_L(\eta(X_L^*)\Theta_{2,L})\|_2 \} \\
&\leq K \mathbb{E}_X \{ \|\eta(X_L^*)\|_2 \|\eta(X_L^*)\Theta_{1,L} - \eta(X_L^*)\Theta_{2,L}\|_2 \} \\
&\leq \underbrace{K \mathbb{E}_X \{ \|\eta(X_L^*)\|_2^2 \}}_{K_2 :=} \|\Theta_{1,L} - \Theta_{2,L}\|_2^2,
\end{aligned}$$

where K_2 has been defined. We repeated used the Cauchy–Schwarz inequality and the last inequality relies on the assumption that ϕ_L is K -Lipschitz continuous.

Note that given random samples $\{X_1, \dots, X_N\}$, the quantities $\mathbb{E}_X \{ \lambda_{\min}(\eta^\top(X_L^*)\eta(X_L^*)) \}$ and $\mathbb{E}_X \{ \|\eta(X_L^*)\|_2^2 \}$ can be empirically approximated by sample averages.

Lastly, when the true signal Θ_L^* is the input to F ,

$$\begin{aligned}
F(\Theta_L^*) &= \mathbb{E}_{X,Y} \{ \eta^\top[\phi_L(\eta(X_L^*)\Theta_L^*) - Y] \} \\
&= \mathbb{E}_{X,Y} \{ \eta^\top(X_L^*)[\phi_L(\eta(X_L^*)\Theta_L^*) - \phi_L(\eta(X_L^*)\Theta_L^*)] \} = 0,
\end{aligned}$$

where we used the fact that $\mathbb{E}[Y|X] = \phi_L(\eta(X_L^*)\Theta_L^*)$. □

Proof of Lemma 4.2. The proof employs classical techniques when analyzing the convergence of projection descent in stochastic optimization, which appear in (Juditsky & Nemirovsky, 2019, Proposition 3.2).

First, for any $\Theta_L \in \Theta$,

$$\begin{aligned}
\mathbb{E}_{(X,Y^{\Theta_L})} \{ \|\eta^\top(X_L^*)\phi(\eta(X_L^*)\Theta_L)\|_2 \} &= \mathbb{E}_X \{ \|\mathbb{E}_{Y^{\Theta_L}} \{ \eta(X_L^*)Y^{\Theta_L} \} \|_2 \} \\
&\leq \mathbb{E}_X \mathbb{E}_{Y^{\Theta_L}} \{ \|\eta(X_L^*)Y^{\Theta_L}\|_2 \} \quad [\text{Jensen's Inequality}] \\
&= \mathbb{E}_{(X,Y^{\Theta_L})} \{ \|\eta(X_L^*)Y^{\Theta_L}\|_2 \} \leq M.
\end{aligned}$$

By the form of F , we then have that $\mathbb{E}_{X,Y} \{ \|F(\Theta_L)\|_2^2 \} \leq 4M^2$ for any Θ_L .

Next, note that each $\hat{\Theta}_L^{(t)}$ is a deterministic function of $Z^N := \{(X_i, Y_i)\}_{i=1}^N$. Define the difference of estimation and its expected value as

$$D_t(Z^N) := \frac{1}{2} \|\hat{\Theta}_L^{(t)} - \Theta_L^*\|_2^2, \quad d_t := \mathbb{E}_{Z^N} \{ D_t(Z^N) \}.$$

As a result,

$$\begin{aligned}
D_t(Z^N) &= \frac{1}{2} \|\text{Proj}_{\Theta} [\hat{\Theta}_L^{(t-1)} - \gamma_t F_{1:N}^T(\hat{\Theta}_L^{(t-1)}) - \Theta_L^*]\|_2^2 \\
&\leq \frac{1}{2} \|\hat{\Theta}_L^{(t-1)} - \gamma_t F_{1:N}^T(\hat{\Theta}_L^{(t-1)}) - \Theta_L^*\|_2^2 \quad [\text{The projection is a contraction}] \\
&= \frac{1}{2} \|\hat{\Theta}_L^{(t-1)} - \Theta_L^*\|_2^2 - \gamma_t F_{1:N}^T(\hat{\Theta}_L^{(t-1)})(\hat{\Theta}_L^{(t-1)} - \Theta_L^*) + \frac{1}{2} \gamma_t^2 \|F_{1:N}^T(\hat{\Theta}_L^{(t-1)})\|_2^2.
\end{aligned}$$

Taking expectation of both sides with respect to Z^N yields

$$\begin{aligned}
d_t &\leq \frac{1}{2} d_{t-1} - \gamma_t \mathbb{E}_{Z^N} [F_{1:N}^T(\hat{\Theta}_L^{(t-1)})(\hat{\Theta}_L^{(t-1)} - \Theta_L^*)] + 2\gamma_t^2 M^2 \\
&\leq (1 - 2\kappa\gamma_t) d_{t-1} + 2\gamma_t^2 M^2,
\end{aligned}$$

where the last inequality follows by noting that $F_{1:N}$ is an unbiased estimator of F , which satisfies

$$F(\Theta_L)^T(\Theta_L - \Theta_L^*) \geq \kappa \|\Theta_L - \Theta_L^*\|_2,$$

due to $F(\Theta_L^*) = 0$. Then, using triangle inequality yields the result.

Lastly, we prove by induction that if we define $R := (2M^2)/\kappa^2$, $\gamma_t := 1/\kappa(t+1)$, we have

$$d_t \leq \frac{R}{t+1}.$$

(Base case when $t = 0$.) Let B be the $\|\cdot\|_2$ diameter of Θ (e.g., $\|\Theta_1 - \Theta_2\|_2^2 \leq B^2 \forall (\Theta_1, \Theta_2) \in \Theta$). Denote $\Theta_L^+, \Theta_L^- \in \mathcal{B}$ to satisfy $\|\Theta_L^+ - \Theta_L^-\|_2^2 = B^2$. By the definition of κ ,

$$\langle F(\Theta_L^+) - F(\Theta_L^-), \Theta_L^+ - \Theta_L^- \rangle \geq \kappa \|\Theta_L^+ - \Theta_L^-\|_2^2 = \kappa B^2.$$

Meanwhile, the Cauchy-Schwarz inequality yields

$$\langle F(\Theta_L^+) - F(\Theta_L^-), \Theta_L^+ - \Theta_L^- \rangle = \langle \eta(X_L^*)(\phi(\eta(X_L^*)))\Theta_L^+ - \eta(X_L^*)(\phi(\eta(X_L^*)))\Theta_L^-, \Theta_L^+ - \Theta_L^- \rangle \leq 2MB.$$

Thus, $B \leq 2M/\kappa$. As a result, $B^2/2 \leq 2M^2/\kappa^2 = R$. Because $d_0 := \|\hat{\Theta}_L^{(0)} - \Theta_L^*\|_2^2 \leq B^2$,

$$d_0 \leq 2R = \frac{4M^2}{\kappa^2}.$$

(The inductive step from $t-1$ to t .) Note that by the definition of γ_t , $\kappa\gamma_t = 1/(t+1) \leq 1/2$. Thus,

$$\begin{aligned}
d_t &\leq (1 - 2\kappa\gamma_t) d_{t-1} + 2\gamma_t^2 M^2 \\
&= \frac{R}{t} \left(1 - \frac{2}{t+1}\right) + \frac{R}{(t+1)^2} \leq \frac{R}{t+1},
\end{aligned}$$

whereby the proof is complete by the definition of d_t and R . □

Proof of Theorem 4.3. Note that when $p = 2$,

$$\begin{aligned}
& \mathbb{E}_{\widehat{\Theta}_L^{(T)}} \{ \|\widehat{\mathbb{E}}[Y_t|X_t] - \mathbb{E}[Y_t|X_t]\|_2 \} \\
&= \mathbb{E}_{\widehat{\Theta}_L^{(T)}} \{ \|\phi(\eta^\top(X_{t,L}^*)\widehat{\Theta}_L^{(T)}) - \phi(\eta^\top(X_{t,L}^*)\Theta_L^*)\|_2 \} \\
&\leq \mathbb{E}_{\widehat{\Theta}_L^{(T)}} \{ K \|\eta^\top(X_{t,L}^*)[\widehat{\Theta}_L^{(T)} - \Theta_L^*]\|_2 \} \\
&\leq K \lambda_{\max}(\eta(X_{t,L}^*)\eta^\top(X_{t,L}^*)) \mathbb{E}_{\widehat{\Theta}_L^{(T)}} \{ \|\widehat{\Theta}_L^{(T)} - \Theta_L^*\|_2 \}.
\end{aligned}$$

We can then use the bound on $\mathbb{E}_{\widehat{\Theta}_L^{(T)}} \{ \|\widehat{\Theta}_L^{(T)} - \Theta_L^*\|_2 \}$ from the previous lemma to complete the proof. In addition, because p -norm is decreasing in p , we have that the bound holds for any $p \in [2, \infty]$. \square

Proof of Corollary 4.4. In the case of the MSE loss,

$$\begin{aligned}
|\widehat{\mathcal{L}}(X_t, Y_t) - \mathcal{L}^*(X_t, Y_t)| &= | \|Y_t - \widehat{\mathbb{E}}[Y_t|X_t]\|_2 - \|Y_t - \mathbb{E}[Y_t|X_t]\|_2 | \\
&= | \|Y_t - \mathbb{E}[Y_t|X_t] + (\mathbb{E}[Y_t|X_t] - \widehat{\mathbb{E}}[Y_t|X_t])\|_2 - \|Y_t - \mathbb{E}[Y_t|X_t]\|_2 | \\
&\leq \| \mathbb{E}[Y_t|X_t] - \widehat{\mathbb{E}}[Y_t|X_t] \|_2.
\end{aligned}$$

When $N > C_t/\epsilon$, Theorem 4.3 guarantees that $\mathbb{E}_{\widehat{\Theta}_L^{(T)}} \{ \|\widehat{\mathbb{E}}[Y_t|X_t] - \mathbb{E}[Y_t|X_t]\|_2 \} \leq \epsilon$. Taking expectation on both sides of the above inequality thus yields the result.

In the case of binary cross-entropy loss, using the definition that $L^*(X_t, Y_{t,i}) = Y_{t,i}^T \ln(E_{t,i}^*) + (\mathbf{1} - Y_{t,i})^T \ln(\mathbf{1} - E_{t,i}^*)$

$$\begin{aligned}
\mathbb{E}_{\widehat{\Theta}_L^{(T)}} \{ |\widehat{\mathcal{L}}(X_t, Y_t) - \mathcal{L}^*(X_t, Y_t)| \} &= \sum_{i=1}^n Y_{t,i}^T \ln \left(\frac{E_{t,i}^*}{\widehat{E}_{t,i}} \right) + (\mathbf{1} - Y_{t,i}^T) \ln \left(\frac{\mathbf{1} - E_{t,i}^*}{\mathbf{1} - \widehat{E}_{t,i}} \right) \\
&\leq \sum_{i=1}^n Y_{t,i}^T \ln \left(\frac{E_{t,i}^*}{E_{t,i}^* - \epsilon} \right) + (\mathbf{1} - Y_{t,i}^T) \ln \left(\frac{\mathbf{1} - E_{t,i}^*}{\mathbf{1} - E_{t,i}^* - \epsilon} \right),
\end{aligned}$$

where the last inequality uses the fact that the function $\ln(a)$ is monotonically increasing on $[0, 1]$ and that we use $p = \infty$ in Theorem 4.3 to guarantee that $\mathbb{E}_{\widehat{\Theta}_L^{(T)}} \{ \|\widehat{\mathbb{E}}[Y_t|X_t] - \mathbb{E}[Y_t|X_t]\|_\infty \} \leq \epsilon$. \square

Proof of Theorem 4.6. The crux is to bound the expected value of the norm of F evaluated at the stochastic OE estimate. This bound results from (Kotsalis et al., 2020, Theorem 3.8), where in general, for any $\Theta_L \in \Theta$, the authors use the residual

$$\mathbb{E}[\text{res}(\Theta_L)] \leq \epsilon, \quad \text{res}(\Theta_L) := \min_{y \in -N_{\Theta}(\Theta_L)} \|y - F(\Theta_L)\|_2$$

as the termination criteria for the recurrence under a certain choice of the Bregman's distance $V(a, b)$; we let $V(a, b) = \|a - b\|_2^2/2$ in our case. The quantity $N_{\Theta}(\Theta_L) := \{y \in \mathbb{R}^p | \langle y, \Theta' - \Theta_L \rangle, \forall \Theta' \in \Theta\}$ denotes the normal cone of Θ at Θ_L . Then, under the assumptions on F and choices of step sizes, we can restate

(Kotsalis et al., 2020, Theorem 3.8) in our special case as

$$\mathbb{E}_{\hat{\Theta}_L^{(R)}}[\text{res}(\hat{\Theta}_L^{(R)})] \leq \frac{3\sigma}{\sqrt{T}} + \frac{12K_2\sqrt{2\|\Theta_L^*\|_2^2 + \frac{2\sigma^2}{L^2}}}{\sqrt{T}}.$$

When we assume Θ is the entire space, $N_{\Theta}(\Theta_L) = \{\mathbf{0}\}$ whereby $\text{res}(\hat{\Theta}_L^{(R)}) = \|F(\hat{\Theta}_L^{(R)})\|_2$. Thus, the result follows.

Furthermore, recall the fact that for any matrix $A \in \mathbb{R}^{m \times n}$ and vectors $x, x' \in \mathbb{R}^n$, we have

$$\|x - x'\|_2 \leq \|A(x - x')\|_2 / \sigma_{\min}(A),$$

where $\sigma_{\min}(A)$ denotes the smallest singular value of A . As a result, by letting $A = \eta(X_L^*), x = \widehat{\mathbb{E}}[Y_t|X_t], x' = \mathbb{E}[Y_t|X_t]$ we have in expectation that

$$\mathbb{E}_{\hat{\Theta}_L^{(R)}}\{\|\mathbb{E}_X\{\sigma_{\min}(\eta(X_L^*))[\widehat{\mathbb{E}}[Y_t|X_t] - \mathbb{E}[Y_t|X_t]]\|_p\} \leq \mathbb{E}_{\hat{\Theta}_L^{(R)}}\|F(\hat{\Theta}_L^{(R)})\|_2,$$

where we used the fact $F(\hat{\Theta}_L^{(R)}) := \mathbb{E}_{X,Y}\{\eta^\top(X_L^*)[\phi_L(\eta(X_L^*)\hat{\Theta}_L^{(R)}) - Y]\} = \mathbb{E}_X\{\eta^\top(X_L^*)[\widehat{\mathbb{E}}[Y_t|X_t] - \mathbb{E}[Y_t|X_t]]\}$. \square

Proof of Proposition 4.7. For notation simplicity, denote $\eta := \eta_L(X_L)$ and $\theta := \Theta_L$. Meanwhile, for two vectors $a, b \in \mathbb{R}^n$, the notation a/b denotes the point-wise division. $\mathbf{1}$ denotes a vector of all 1.

We first consider the binary cross-entropy loss $\mathcal{L}(Y, \Theta_L)$ defined in (10). Note that we have

$$\begin{aligned} \mathcal{L}(Y, \Theta_L) &= -Y \ln(\phi(\eta_L(X_L)\Theta_L)) - (1 - Y) \ln(1 - \phi(\eta_L(X_L)\Theta_L)) \\ &= -Y^T \ln(\exp(\eta\theta)/(\mathbf{1} + \exp(\eta\theta))) - (\mathbf{1} - Y)^T \ln(\mathbf{1}/(\mathbf{1} + \exp(\eta\theta))) \\ &= -Y^T \eta\theta + Y^T \ln(\mathbf{1} + \exp(\eta\theta)) + (\mathbf{1} - Y)^T \ln(\mathbf{1} + \exp(\eta\theta)) \\ &= \mathbf{1}^T \ln(\mathbf{1} + \exp(\eta\theta)) - Y^T \eta\theta. \end{aligned}$$

Thus, the gradient with respect to θ (which is Θ_L) can be written as

$$\nabla_{\theta} \mathcal{L}(Y, \Theta_L) = \eta^T \frac{\exp(\eta\theta)}{\mathbf{1} + \exp(\eta\theta)} - \eta^T Y = \eta_L^\top(X_L)[\phi(\eta_L(X_L)\Theta_L) - Y].$$

Taking expectation thus yields the result.

We next consider the categorical cross-entropy loss $\mathcal{L}(Y, \Theta_L)$ defined in (11). Note that we have

$$\begin{aligned} \mathcal{L}(Y, \Theta_L) &= -e_Y^T \ln(\phi(\eta_L(X_L)\Theta_L)) \\ &= \left[-e_Y^T \ln \left(\frac{\exp(\eta\theta)}{\mathbf{1}^T \exp(\eta\theta)} \right) \right] \\ &= -e_Y^T(\eta\theta) + \ln(\mathbf{1}^T \exp(\eta\theta)). \end{aligned}$$

Thus, the gradient with respect to θ can be written as

$$\begin{aligned}\nabla_{\theta}\mathcal{L}(Y, \Theta) &= -\eta^T e_Y + \eta^T \frac{\exp(\eta\theta)}{\mathbf{1}^T \exp(\eta\theta)} \\ &= \eta^T [\phi(\eta\theta) - e_Y] = \eta_L^T(X_L) [\phi(\eta_L(X_L)\Theta_L) - Y],\end{aligned}$$

where in the definition of $F(\Theta)$ in (4), $Y = e_Y \in \mathbb{R}^{F+1}$ if Y belongs to more than 2 classes. Taking expectation thus yields the result. \square

Proof of Proposition 4.8. Note that we are equivalently showing that there exists $\Theta_{L'}^*$ such that

$$\|\mathbb{E}_X[\phi(L'_g X \Theta_{L'}^*) - \phi(L_g X \Theta_L^*)]\|_2 \leq \epsilon \|\Theta_L^*\|_2.$$

Because $\Theta_{L'}^*$ is the minimizer of ℓ_2 error, it is clear that

$$\mathbb{E}_X[\phi(L'_g X \Theta_{L'}^*) - \phi(L_g X \Theta_L^*)]\|_2 \leq \mathbb{E}_X[\phi(L'_g X \Theta_L^*) - \phi(L_g X \Theta_L^*)]\|_2.$$

Now,

$$\begin{aligned}\|\mathbb{E}_X[\phi(L'_g X \Theta_L^*) - \phi(L_g X \Theta_L^*)]\|_2 &\leq \mathbb{E}_X\|\phi(L'_g X \Theta_L^*) - \phi(L_g X \Theta_L^*)\|_2 \\ &\leq K \mathbb{E}_X\|L'_g X \Theta_L^* - L_g X \Theta_L^*\|_2 \\ &\leq K \mathbb{E}_X\|(L'_g - L_g)X\|_2 \|\Theta_L^*\|_2. \\ &= K \mathbb{E}_X\|(L'_g - L_g)X^-\|_2 \|\Theta_L^*\|_2. \quad \text{Orthogonality of eigenvectors} \\ &\leq K \|L_g^- - L_{g'}^-\|_2 \mathbb{E}_X\|X^-\|_2 \|\Theta_L^*\|_2 \\ &\leq \epsilon \|\Theta_L^*\|_2.\end{aligned}$$

Therefore, the loss under the true parameter Θ_L^* is bounded above by $\epsilon \|\Theta_L^*\|_2$, so there exists a $\Theta_{L'}^*$ that achieves no larger error. \square

B Additional Experiments

We show additional results that illustrate the behavior of SVI and SGD during the entire training epoch.

B.1 One-layer model recovery and prediction

One-layer GCN model with sigmoid activation. We use the small graph mentioned in Section 5.3.3. (see Figure 10a for graph visualization) and the only difference is that there is no hidden layer, so that $\mathbb{E}[Y_i|X_i, \Theta_i] = \phi(\eta(X_i)\Theta)$, where $\eta(X)$ filters the graph signal with GCN and ϕ is the sigmoid function. We verified in Proposition 4.7 that SVI is identical to SGD in this model, so that we only show the results for SVI in Figure 8.

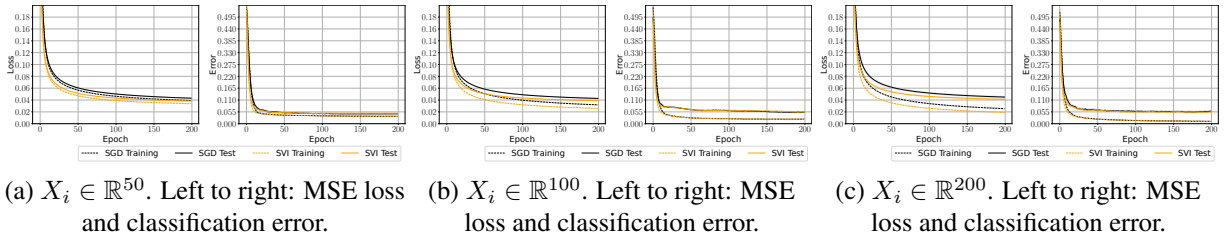
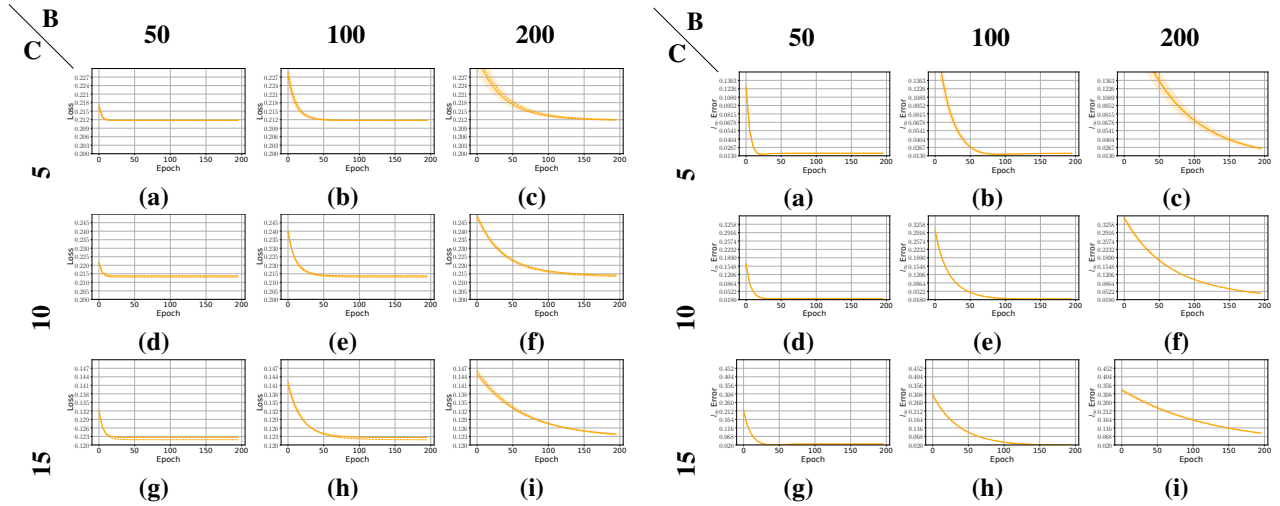


Figure 7: Non-convex one-layer probit model for different feature dimensions over all training epochs. Results are plotted with one standard error bars. In particular, SVI exhibits faster convergence than SGD and reaches smaller errors consistently. Metrics are defined in (12) and (14) respectively.



MSE loss by C and B . The metric is defined in (12). Orange solid (dash) lines denote SVI test (training) results.

ℓ_∞ model recovery error by C and B . The metric is defined in (16). Orange solid (dash) lines denote SVI test (training) results.

Figure 8: One-layer GCN model recovery prediction with the sigmoid activation. C is the in-channel dimension of each node feature $X_{i,n}$, with binary node outputs $Y_{i,n}$. We see that the when the input feature dimension C is fixed, SVI nearly converges to the same MSE loss and the same ℓ_∞ error regardless of the batch size B . The differences are only caused by the fewer number of iterations when B increases.

B.2 Two-layer FC networks and GCN

We briefly explain what each figure or table in this section contains. Figure 9 shows model intermediate convergence results for the FC networks. Figure 10 visualizes the small and large random graphs. Table 6 and Figure 11 shows additional results regarding model recovery on the small random graph. Figure 12 shows intermediate convergence results on both small and large random graphs. Tables 7 and 8 show the sensitivity of SVI and SGD to changes in batches sizes, without and with BN, and Figures 13 and 14 show the corresponding intermediate convergence results. In particular, we will present a detailed qualitative analyses of results on the sensitivity of SVI and SGD to changes in batches sizes, without and with BN.

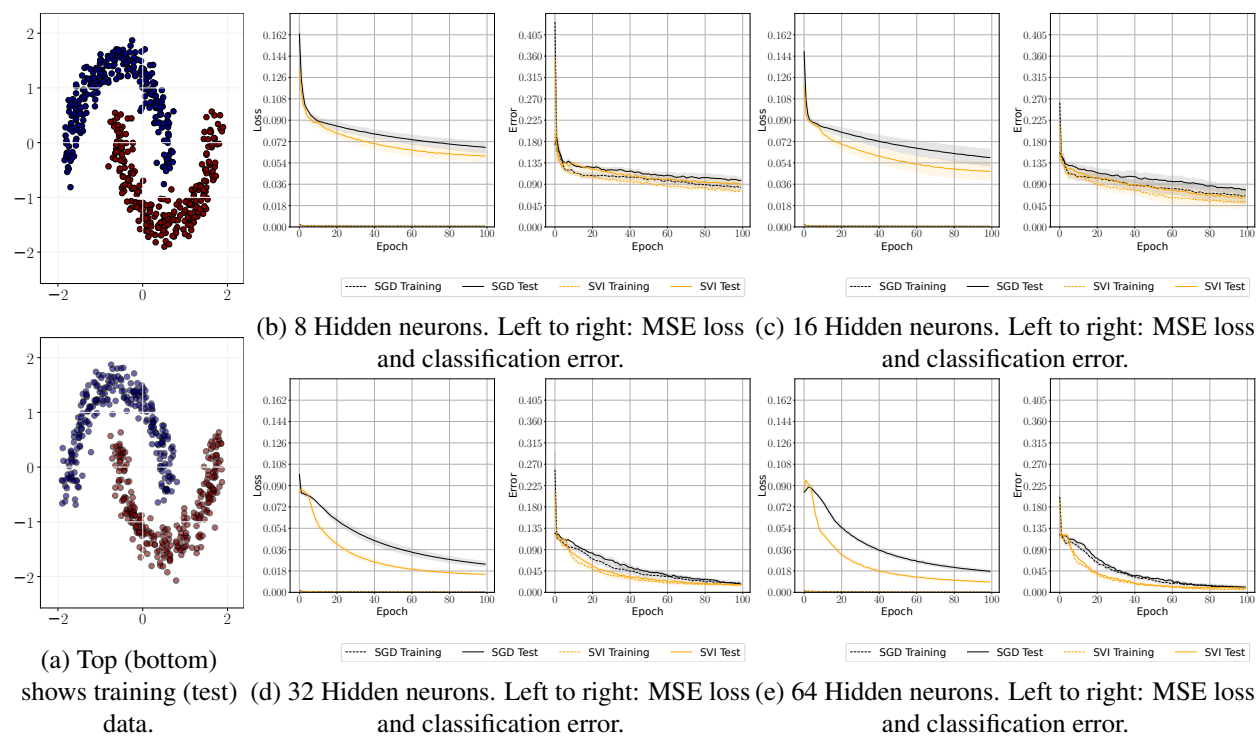


Figure 9: Two-moon FC network. Results are plotted with one standard error bars. In particular, SVI exhibits faster convergence than SGD and shows smaller errors. Metrics are defined in (12) and (14) respectively.

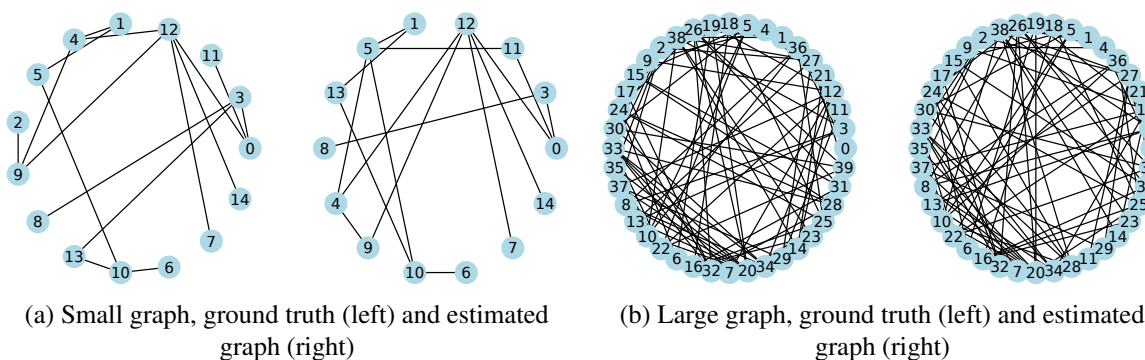


Figure 10: Illustration of small and random graphs.

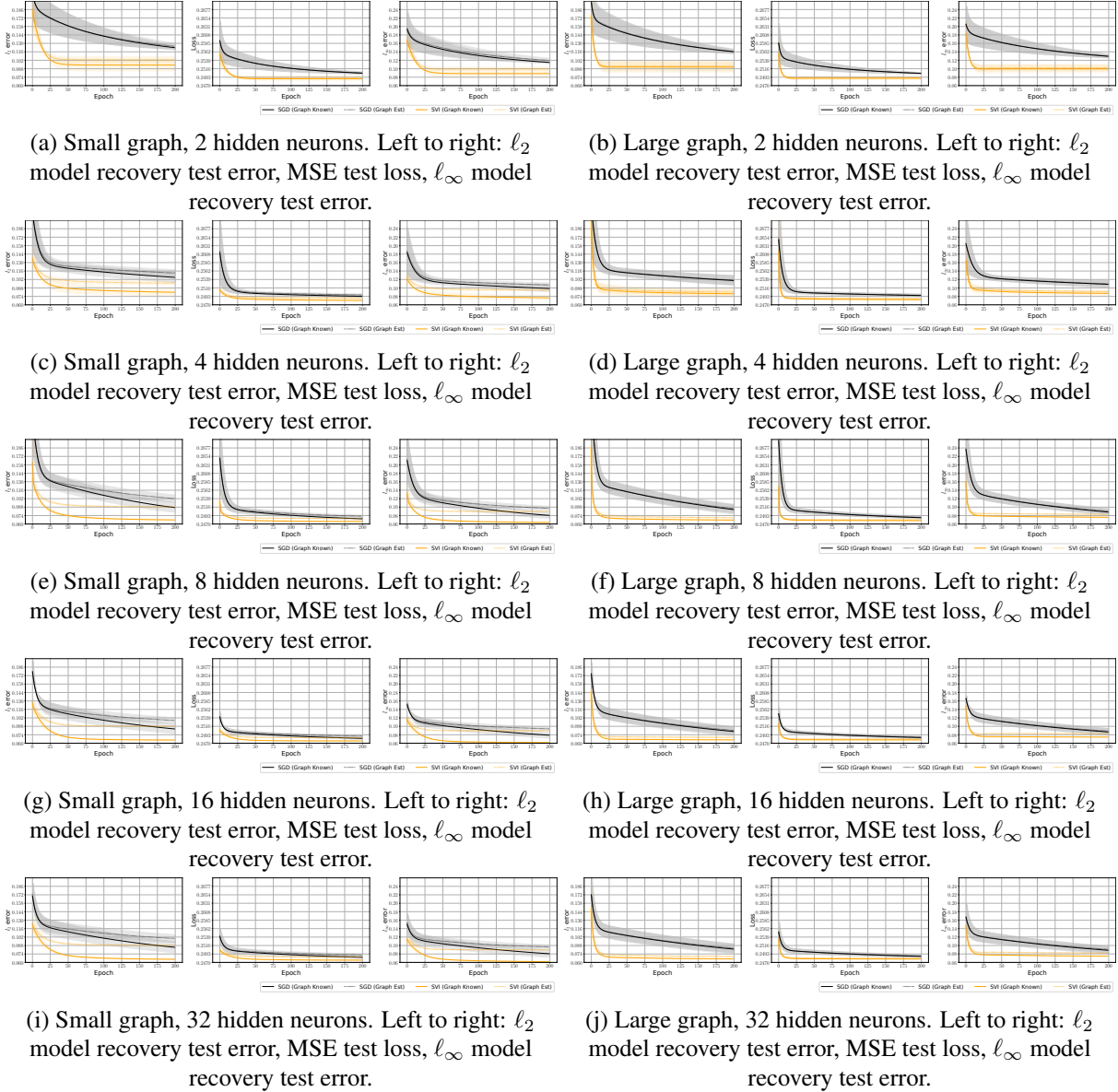


Figure 12: Two-layer GCN model recovery and prediction on small (left column) or large (left column) graphs. We compare SGD vs. SVI under different numbers of hidden neurons with $B = 100$. SVI consistently reaches smaller error with faster convergence. Metrics are defined in (12) and (16) respectively.

Small Graph # Hidden neurons	ℓ_2 model recovery test error				MSE test loss				ℓ_∞ model recovery test error			
	SGD (Known)	SGD (Perturbed)	SVI (Known)	SVI (Perturbed)	SGD (Known)	SGD (Perturbed)	SVI (Known)	SVI (Perturbed)	SGD (Known)	SGD (Perturbed)	SVI (Known)	SVI (Perturbed)
2	0.123 (3.3e-03)	0.125 (4.9e-03)	0.094 (9.7e-03)	0.103 (5.4e-03)	0.25 (2.3e-04)	0.25 (3.0e-04)	0.249 (4.4e-04)	0.249 (3.0e-04)	0.115 (2.9e-03)	0.12 (4.9e-03)	0.089 (8.9e-03)	0.1 (3.9e-03)
4	0.105 (8.7e-03)	0.113 (5.5e-03)	0.081 (5.8e-03)	0.096 (2.8e-03)	0.249 (3.9e-04)	0.25 (2.8e-04)	0.248 (2.1e-04)	0.249 (1.4e-04)	0.099 (7.9e-03)	0.107 (4.4e-03)	0.077 (5.3e-03)	0.095 (1.8e-03)
8	0.087 (8.0e-03)	0.102 (5.8e-03)	0.067 (5.6e-04)	0.088 (1.3e-04)	0.248 (3.2e-04)	0.249 (2.6e-04)	0.248 (2.1e-05)	0.249 (2.3e-05)	0.081 (7.2e-03)	0.097 (4.7e-03)	0.064 (6.4e-04)	0.09 (1.6e-04)
16	0.084 (7.7e-03)	0.098 (4.6e-03)	0.065 (4.0e-04)	0.088 (1.5e-04)	0.248 (2.9e-04)	0.249 (2.1e-04)	0.248 (7.0e-06)	0.248 (2.5e-05)	0.079 (7.1e-03)	0.094 (3.4e-03)	0.062 (3.3e-04)	0.09 (1.3e-04)
32	0.085 (9.2e-03)	0.1 (6.2e-03)	0.065 (4.3e-04)	0.088 (3.6e-04)	0.248 (4.1e-04)	0.249 (3.3e-04)	0.248 (2.3e-05)	0.248 (3.8e-05)	0.081 (8.4e-03)	0.096 (4.8e-03)	0.062 (5.0e-04)	0.09 (1.3e-04)

Table 6: Two-layer GCN model recovery on the small random graph, with identical learning rate and ReLU activation for both SVI and SGD under $B = 100$. We measure recovery performance according to relative errors in predicting the posterior probability $\mathbb{E}[Y_i|X_i]$ on test data. The middle column shows the MSE loss on test data. We observe consistently better model recovery performance by SVI, regardless of the number of hidden neurons for estimation, comparison metrics, and whether graph is perturbed. Metrics are defined in (16) and (12) respectively.

Sensitivity of SVI and SGD under batch size and/or batch normalization. Overall, when no BN acceleration is used, SGD converges much more slowly than SVI. Hence, we adopt BN for both SVI and SGD. We first remark the following modification to SVI in Algorithm 1 under BN. Originally, we have after layer l

$$X_{l+1} := \phi_L(\eta(X_l)\Theta_l),$$

where ϕ_L is the activation function and $\eta(X_l)$ is the hidden feature representation at layer l , filtered by the graph operator $\eta(\cdot)$. Under batch normalization, we have

$$X_{l+1} := \phi_L(\text{BN}(\eta(X_l)\Theta_l)), \quad (17)$$

where $\text{BN}(X) := (X - \mu(X))/\sigma(X) * \gamma + \beta$. For simplicity, we assume $\gamma = \mathbf{1}, \beta = \mathbf{0}$ but can also treat them as learnable parameters. In addition, denote $\hat{\mu}$ and $\hat{\sigma}$ as the estimates for $\mu(X)$ and $\sigma(X)$ given any batch.

Now, when $\eta(X_l)\Theta_l = L_g X_l W_l + b_l$, where L_g denotes the graph filter, $\text{BN}(\eta(X_l)\Theta_l)$ in (17) becomes

$$\begin{aligned} \text{BN}(\eta(X_l)\Theta_l) &= [(L_g X_l W_l + b_l) - \hat{\mu}]/\hat{\sigma} \\ &= L_g X_l \underbrace{W_l/\hat{\sigma}}_{\widetilde{W}_l} + \underbrace{(b_l - \hat{\mu})/\hat{\sigma}}_{\widetilde{b}_l}. \end{aligned}$$

Thus, the gradients in line 5 or 6 of Algorithm 1 are update directions for \widetilde{W}_l and \widetilde{b}_l . We thus need to additionally multiply the gradients by $\hat{\sigma}$ so that they are update directions for W_l and b_l .

In addition, we found in practice that “freezing” BN sometime during training further accelerates SGD, so we also adopt these additional techniques. In particular, we freeze the running mean and variance in BN after training SGD or SVI for 50% of total epochs and use these frozen values for further normalization during training. Hence, the *best-of-three* result refers to the smallest MSE error or ℓ_p model recovery error

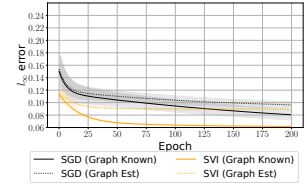


Figure 11: ℓ_∞ model recovery error on the small random graph. SVI consistently reaches smaller error under faster convergence, even just after the first training epoch.

under these three approaches (i.e., no BN, BN, and half-frozen BN).

We now present a detailed qualitative analyses of Tables 7 (no BN, final results) and 8 (best of three, final results), as well as Figures 13 and 14 regarding intermediate convergence.

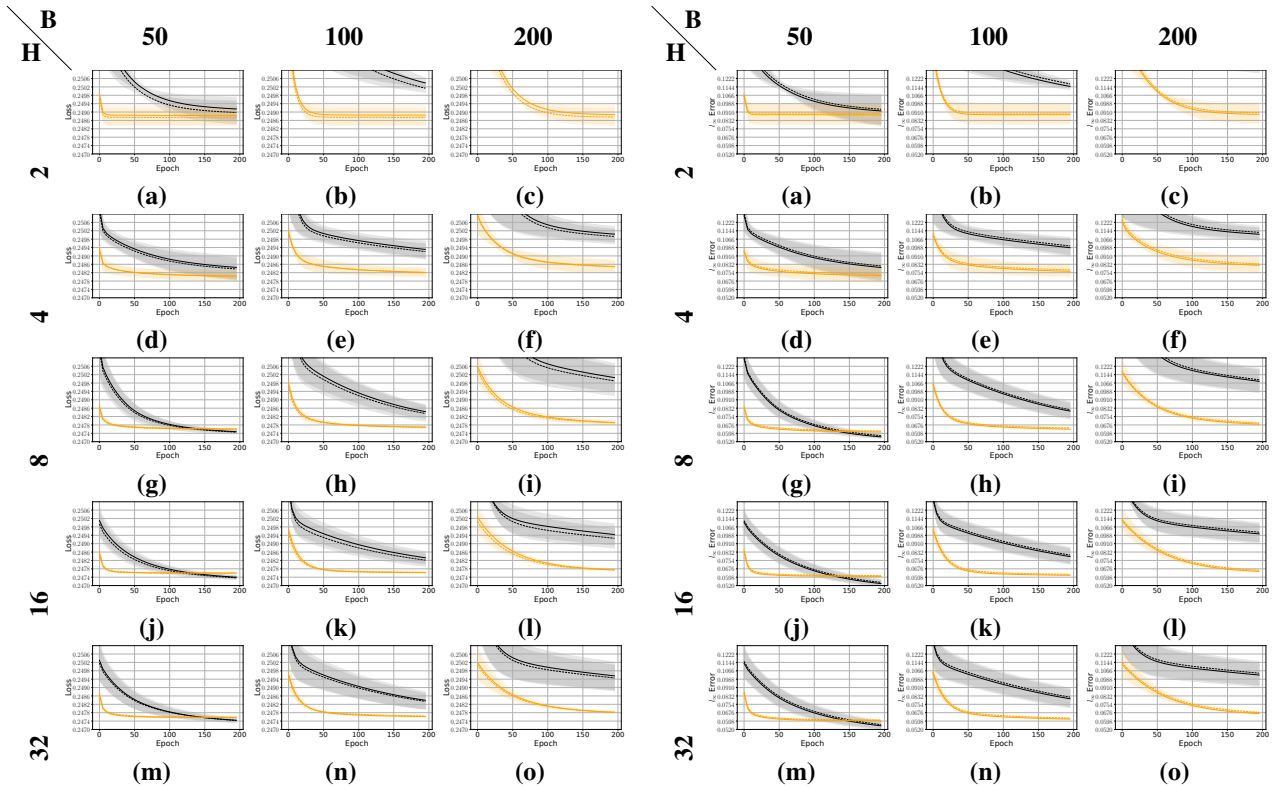
- In terms of the final MSE error in both tables, both SGD and SVI yield very similar training and test results in the range of $0.246 \sim 0.249$, regardless of normalization, H , or B .
- In terms of the final ℓ_∞ model recovery error:
 - (1) When no BN is used (see Table 7), SVI yields significantly smaller error than SGD when $B = 100$ or 200 regardless of H (e.g., 0.08 vs. 0.06). When $B = 50$, SGD may yield smaller final error than SVI when the network is more over-parametrized (e.g., $H = 8, 16, 32$), but the difference is less significant (e.g., 0.056 vs. 0.061). Moreover, at a fixed H , SVI is much less sensitive to the change in B (not so for SGD) and in general, SVI with $H = 8, B = 50$ reaches much better performance than SGD with $H = 32, B = 50$ or 100 and reaches competitive performance as SGD with $H = 8/16/32, B = 50$.
 - (2) When the best of three normalization approaches is chosen (see Table 8), if $B = 100$ or 200, SVI still reaches significantly smaller ℓ_∞ error under the majority of H values and either full or half-way BN can improve SVI performance. When $B = 50$, SVI is still very competitive or better than SGD when $H = 2, 4, 8$. Interestingly, SVI yields higher error when H increases beyond 8 hidden neurons. In addition, if $H = 2, 4, 8$, SVI is still insensitive to changes in B (not so for SGD) and in particular SVI with $H = 8, B = 100$ reaches the second smallest test error across all combinations for SGD and SVI.
- In terms of the intermediate convergence (see Figure 13 and 14), SVI almost always reaches much lower MSE loss or ℓ_∞ error than SGD at the first few epochs. In particular, running SVI for one epoch may already yield very small loss or error comparing to SGD.

H	$B = 50$				$B = 100$				$B = 200$				$B = 50$				$B = 100$				$B = 200$							
	MSE loss				MSE loss				MSE loss				ℓ_∞ model recovery error				ℓ_∞ model recovery error				ℓ_∞ model recovery error							
	SGD train	SGD test	SVI train	SVI test	SGD train	SGD test	SVI train	SVI test	SGD train	SGD test	SVI train	SVI test	SGD train	SGD test	SVI train	SVI test	SGD train	SGD test	SVI train	SVI test	SGD train	SGD test	SVI train	SVI test	SGD train	SGD test	SVI train	SVI test
2	0.2490 (5.4e-04)	0.2491 (5.6e-04)	0.2487 (3.8e-04)	0.2488 (4.3e-04)	0.2501 (2.0e-04)	0.2504 (2.4e-04)	0.2487 (3.9e-04)	0.2489 (4.4e-04)	0.2525 (1.4e-03)	0.2528 (1.5e-03)	0.2488 (3.9e-04)	0.2489 (4.4e-04)	0.0936 (1.4e-02)	0.0921 (1.4e-02)	0.0899 (9.1e-03)	0.0884 (8.9e-03)	0.1172 (3.1e-03)	0.1148 (2.9e-03)	0.0901 (9.1e-03)	0.0885 (8.9e-03)	0.1461 (1.6e-02)	0.1432 (1.6e-02)	0.0904 (9.0e-03)	0.0889 (8.9e-03)	0.1461 (1.6e-02)	0.1432 (1.6e-02)	0.0904 (9.0e-03)	0.0889 (8.9e-03)
4	0.2484 (5.2e-04)	0.2485 (5.5e-04)	0.2480 (2.4e-04)	0.2480 (2.4e-04)	0.2492 (3.6e-04)	0.2493 (3.9e-04)	0.2482 (1.8e-04)	0.2482 (2.1e-04)	0.2499 (3.4e-04)	0.2500 (3.6e-04)	0.2485 (2.7e-04)	0.2485 (3.1e-04)	0.0817 (1.2e-02)	0.0802 (1.2e-02)	0.0739 (6.7e-03)	0.0726 (6.5e-03)	0.1003 (7.9e-03)	0.0986 (7.9e-03)	0.0780 (5.4e-03)	0.0767 (5.3e-03)	0.1129 (5.8e-03)	0.1112 (5.7e-03)	0.0836 (7.0e-03)	0.0822 (7.0e-03)	0.1129 (5.8e-03)	0.1112 (5.7e-03)	0.0836 (7.0e-03)	0.0822 (7.0e-03)
8	0.2475 (9.0e-05)	0.2475 (4.6e-05)	0.2476 (3.5e-05)	0.2476 (1.3e-05)	0.2483 (3.7e-04)	0.2484 (3.2e-04)	0.2477 (4.5e-05)	0.2477 (2.1e-05)	0.2499 (6.9e-04)	0.2501 (6.7e-04)	0.2479 (8.6e-05)	0.2479 (7.9e-05)	0.0576 (1.6e-03)	0.0565 (1.5e-03)	0.0619 (3.7e-04)	0.0610 (3.9e-04)	0.0818 (7.3e-03)	0.0805 (7.2e-03)	0.0648 (6.3e-04)	0.0637 (6.4e-04)	0.1096 (1.1e-02)	0.1082 (1.0e-02)	0.0693 (1.5e-03)	0.0683 (1.5e-03)	0.1096 (1.1e-02)	0.1082 (1.0e-02)	0.0693 (1.5e-03)	0.0683 (1.5e-03)
16	0.2474 (9.3e-05)	0.2474 (6.2e-05)	0.2476 (2.6e-05)	0.2476 (6.4e-06)	0.2482 (2.9e-04)	0.2483 (2.9e-04)	0.2476 (2.9e-05)	0.2476 (6.9e-06)	0.2493 (4.7e-04)	0.2494 (5.0e-04)	0.2477 (5.4e-05)	0.2478 (3.1e-05)	0.0550 (2.9e-03)	0.0539 (2.8e-03)	0.0613 (9.6e-05)	0.0605 (1.0e-04)	0.0804 (7.1e-03)	0.0790 (7.1e-03)	0.0625 (3.4e-04)	0.0616 (3.3e-04)	0.1017 (8.8e-03)	0.1001 (8.7e-03)	0.0663 (9.3e-04)	0.0651 (8.6e-04)	0.1017 (8.8e-03)	0.1001 (8.7e-03)	0.0663 (9.3e-04)	0.0651 (8.6e-04)
32	0.2474 (6.9e-05)	0.2474 (1.1e-04)	0.2476 (2.2e-05)	0.2476 (1.0e-05)	0.2483 (3.7e-04)	0.2484 (4.1e-04)	0.2476 (1.1e-05)	0.2476 (2.3e-05)	0.2495 (6.1e-04)	0.2496 (6.6e-04)	0.2478 (1.9e-05)	0.2478 (5.0e-05)	0.0565 (3.5e-03)	0.0554 (3.4e-03)	0.0608 (2.8e-04)	0.0601 (2.4e-04)	0.0821 (8.4e-03)	0.0806 (8.4e-03)	0.0626 (5.3e-04)	0.0617 (5.0e-04)	0.1044 (1.1e-02)	0.1027 (1.1e-02)	0.0680 (8.1e-04)	0.0667 (7.9e-04)	0.1044 (1.1e-02)	0.1027 (1.1e-02)	0.0680 (8.1e-04)	0.0667 (7.9e-04)

Table 7: Two-layer GCN model recovery and prediction without BN at the end of epochs. See the bullet points above for detailed qualitative analyses. Metrics are defined in (12) and (16) respectively.

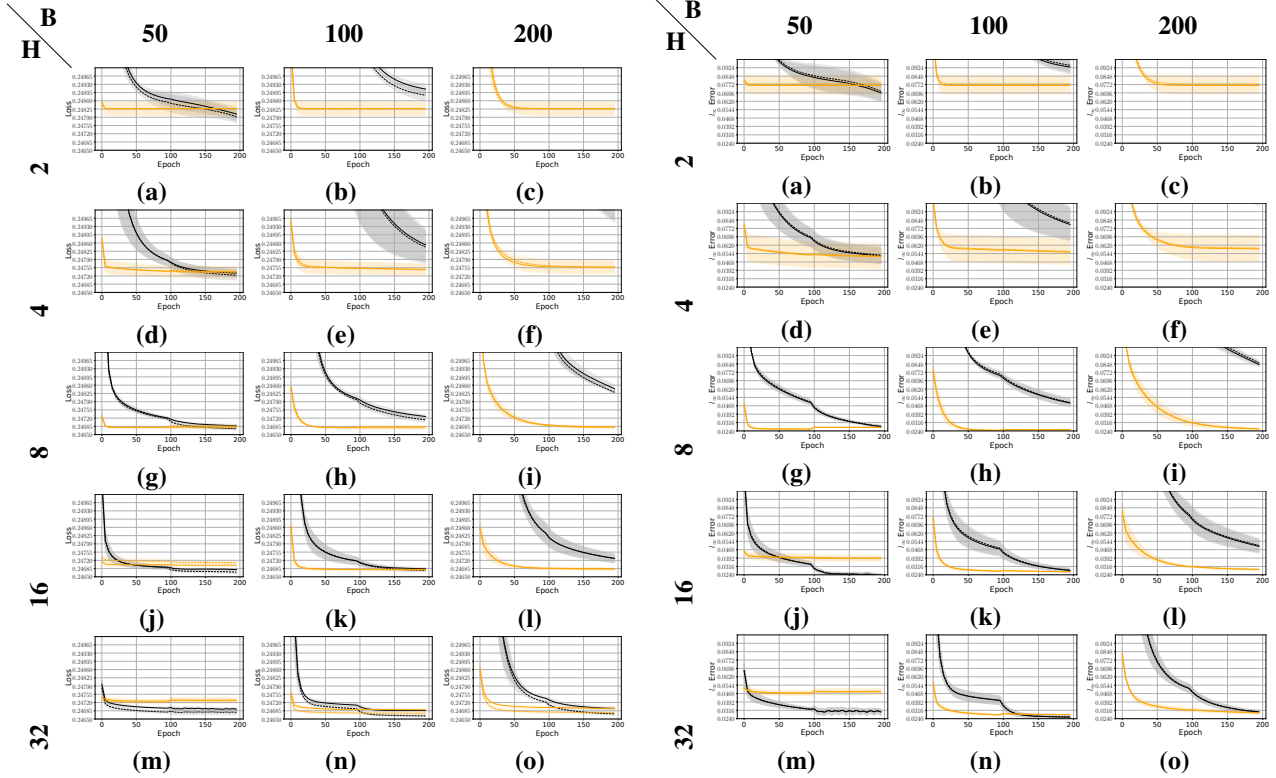
H	$B = 50$				$B = 100$				$B = 200$				$B = 50$				$B = 100$				$B = 200$						
	MSE loss				MSE loss				MSE loss				ℓ_∞ model recovery error				ℓ_∞ model recovery error				ℓ_∞ model recovery error						
	SGD train	SGD test	SVI train	SVI test	SGD train	SGD test	SVI train	SVI test	SGD train	SGD test	SVI train	SVI test	SGD train	SGD test	SVI train	SVI test	SGD train	SGD test	SVI train	SVI test	SGD train	SGD test	SVI train	SVI test	SGD train	SGD test	SVI train
2	0.2479 (2.5e-04)	0.2480 (2.8e-04)	0.2483 (2.5e-04)	0.2483 (2.9e-04)	0.2488 (2.4e-04)	0.2491 (2.0e-04)	0.2483 (2.5e-04)	0.2483 (2.9e-04)	0.2524 (5.3e-04)	0.2527 (5.3e-04)	0.2483 (4.4e-04)	0.2483 (2.8e-04)	0.0711 (8.4e-03)	0.0697 (8.2e-03)	0.0777 (0.3)	0.0764 (8.0e-03)	0.0947 (6.3e-03)	0.0931 (6.1e-03)	0.0777 (8.3e-03)	0.0764 (8.1e-03)	0.1461 (1.6e-02)	0.1432 (1.6e-02)	0.0777 (8.3e-03)	0.0763 (8.0e-03)			
4	0.2472 (2.0e-04)	0.2473 (1.7e-04)	0.2473 (2.6e-04)	0.2474 (2.2e-04)	0.2484 (6.8e-04)	0.2485 (7.1e-04)	0.2475 (2.5e-04)	0.2475 (2.2e-04)	0.2499 (3.4e-04)	0.2500 (3.6e-04)	0.2476 (2.8e-04)	0.2476 (2.6e-04)	0.0530 (7.4e-03)	0.0523 (7.0e-03)	0.0517 (0.2)	0.0510 (0.2)	0.0820 (1.5e-02)	0.0808 (1.4e-02)	0.0559 (1.2e-02)	0.0552 (1.1e-02)	0.1129 (5.8e-03)	0.1112 (5.7e-03)	0.0593 (1.2e-02)	0.0585 (1.2e-02)			
8	0.2468 (5.1e-05)	0.2469 (5.7e-05)	0.2468 (5.3e-05)	0.2468 (3.6e-05)	0.2471 (9.4e-05)	0.2473 (6.9e-05)	0.2468 (5.0e-05)	0.2468 (3.2e-05)	0.2483 (6.2e-05)	0.2484 (1.5e-05)	0.2468 (5.0e-05)	0.2468 (2.9e-05)	0.0282 (1.2e-03)	0.0279 (1.3e-03)	0.0257 (4.2e-04)	0.0258 (4.4e-04)	0.0498 (3.5e-03)	0.0493 (3.4e-03)	0.0242 (2.6e-03)	0.0242 (2.5e-03)	0.0858 (2.0e-03)	0.0842 (2.1e-03)	0.0257 (0.3)	0.0256 (0.4)			
16	0.2467 (5.8e-05)	0.2468 (2.5e-05)	0.2471 (5.3e-05)	0.2470 (5.8e-05)	0.2468 (6.7e-05)	0.2468 (5.7e-05)	0.2468 (3.6e-05)	0.2468 (3.1e-05)	0.2473 (1.9e-04)	0.2473 (1.7e-04)	0.2468 (4.4e-05)	0.2468 (4.9e-05)	0.0238 (1.3e-03)	0.0237 (1.3e-03)	0.0387 (2.3e-03)	0.0392 (2.4e-03)	0.0283 (1.9e-03)	0.0279 (1.9e-03)	0.0262 (3.9e-04)	0.0262 (4.4e-04)	0.0507 (6.3e-03)	0.0498 (6.1e-03)	0.0287 (0.3)	0.0286 (0.4)			
32	0.2468 (5.1e-05)	0.2469 (6.2e-05)	0.2472 (8.6e-05)	0.2473 (7.7e-05)	0.2466 (4.0e-05)	0.2469 (5.0e-05)	0.2467 (4.1e-05)	0.2469 (2.4e-05)	0.2467 (5.6e-05)	0.2469 (7.2e-05)	0.2468 (5.0e-05)	0.2469 (3.7e-05)	0.0295 (6.5e-04)	0.0295 (5.8e-04)	0.0471 (1.8e-03)	0.0475 (1.9e-03)	0.0255 (1.5e-03)	0.0254 (1.5e-03)	0.0268 (1.7e-03)	0.0268 (2.3e-03)	0.0302 (1.5e-03)	0.0301 (1.6e-03)	0.0290 (0.3)	0.0290 (1.0e-03)			

Table 8: Two-layer GCN model recovery and prediction for the best-of-three result at the end of epochs. See the bullet points before Table 7 for detailed qualitative analyses. Metrics are defined in (12) and (16) respectively.



MSE loss by H and B . The metric is defined in (12). Black (orange) solid (dash) lines denote SGD (SVI) test (training) results. ℓ_∞ error by H and B . The metric is defined in (16). Black (orange) solid (dash) lines denote SGD (SVI) test (training) results.

Figure 13: Two-layer GCN model recovery and prediction without BN regarding intermediate convergence. See the bullet points before Table 7 for detailed qualitative analyses. Some curves miss initial values because they are too large under the shared y-ticks. Metrics are defined in (12) and (16) respectively.



MSE loss by H and B . The metric is defined in (12). Black (orange) solid (dash) lines denote SGD (SVI) test (training) results.

ℓ_∞ model recovery error by H and B . The metric is defined in (16). Black (orange) solid (dash) lines denote SGD (SVI) test (training) results.

Figure 14: Two-layer GCN model recovery and prediction under half-frozen BN regarding intermediate convergence. We found that half-frozen BN generally further accelerates BN. See the bullet points before Table 7 for detailed qualitative analyses. Some curves miss initial values because they are too large under the shared y-ticks. Metrics are defined in (12) and (16) respectively.

B.3 Three-layer real data

Solar data. Data are retrieved from <https://nstrdb.nrel.gov/>. We first show results for the Los-Angeles solar data, and then provide the complete results that demonstrate the behavior of both methods over epochs, without and with BN.

Los-Angeles solar data	MSE loss				Classification error				Weighted F_1 score			
	# Hidden neurons	SGD Training	SGD Test	SVI Training	SVI Test	SGD Training	SGD Test	SVI Training	SVI Test	SGD Training	SGD Test	SVI Training
8	0.222 (5.1e-03)	0.219 (5.1e-03)	0.199 (4.0e-03)	0.199 (5.0e-03)	0.32 (1.2e-02)	0.285 (8.6e-03)	0.295 (2.7e-03)	0.287 (1.3e-02)	0.676 (1.4e-02)	0.71 (9.9e-03)	0.705 (3.0e-03)	0.713 (1.3e-02)
16	0.223 (6.6e-03)	0.221 (6.7e-03)	0.195 (7.1e-03)	0.195 (7.2e-03)	0.311 (2.0e-02)	0.307 (1.9e-02)	0.3 (1.1e-02)	0.296 (2.2e-02)	0.683 (2.4e-02)	0.686 (2.1e-02)	0.701 (1.1e-02)	0.704 (2.2e-02)
32	0.225 (1.1e-03)	0.221 (1.6e-03)	0.189 (3.8e-03)	0.186 (2.9e-03)	0.316 (1.3e-02)	0.283 (1.2e-02)	0.272 (1.1e-02)	0.254 (1.2e-02)	0.68 (1.3e-02)	0.711 (1.3e-02)	0.729 (1.1e-02)	0.746 (1.2e-02)
64	0.21 (1.5e-03)	0.207 (1.1e-03)	0.178 (2.9e-04)	0.178 (1.0e-03)	0.27 (1.2e-02)	0.264 (1.1e-02)	0.251 (1.3e-03)	0.258 (6.3e-03)	0.731 (1.2e-02)	0.734 (1.2e-02)	0.748 (1.3e-03)	0.742 (6.3e-03)

Table 9: Los-Angeles solar binary ramping event detection under a three-layer GCN model. In addition to MSE loss and classification loss, we also use the weighted F_1 score as an additional metric, which weighs F_1 score in each class by its support. SVI consistently outperforms SGD on all these metrics on both training and test data.

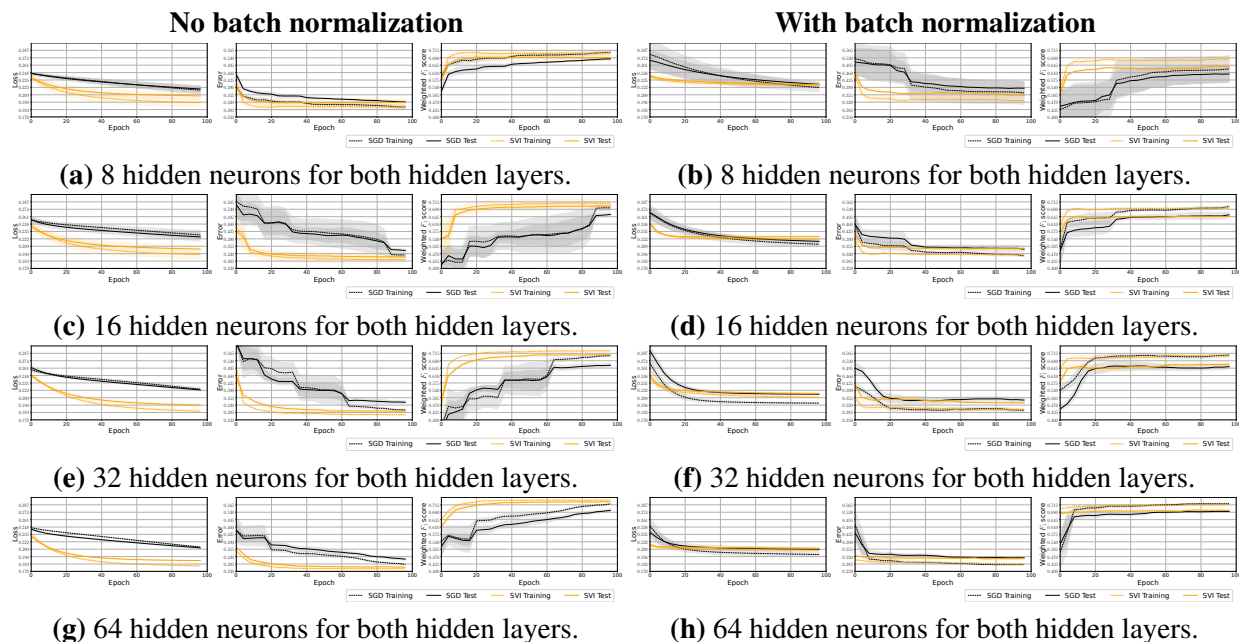


Figure 15: California solar binary ramping event detection under a three-layer GCN model. Left to right in each three-column figure: MSE loss, classification error, and weighted F_1 score. SVI shows faster convergence and smaller errors. In addition, SVI with BN can be worse than SVI without it, and SGD with BN is better than not SGD without it, but SVI without BN still performs the best among the combinations.

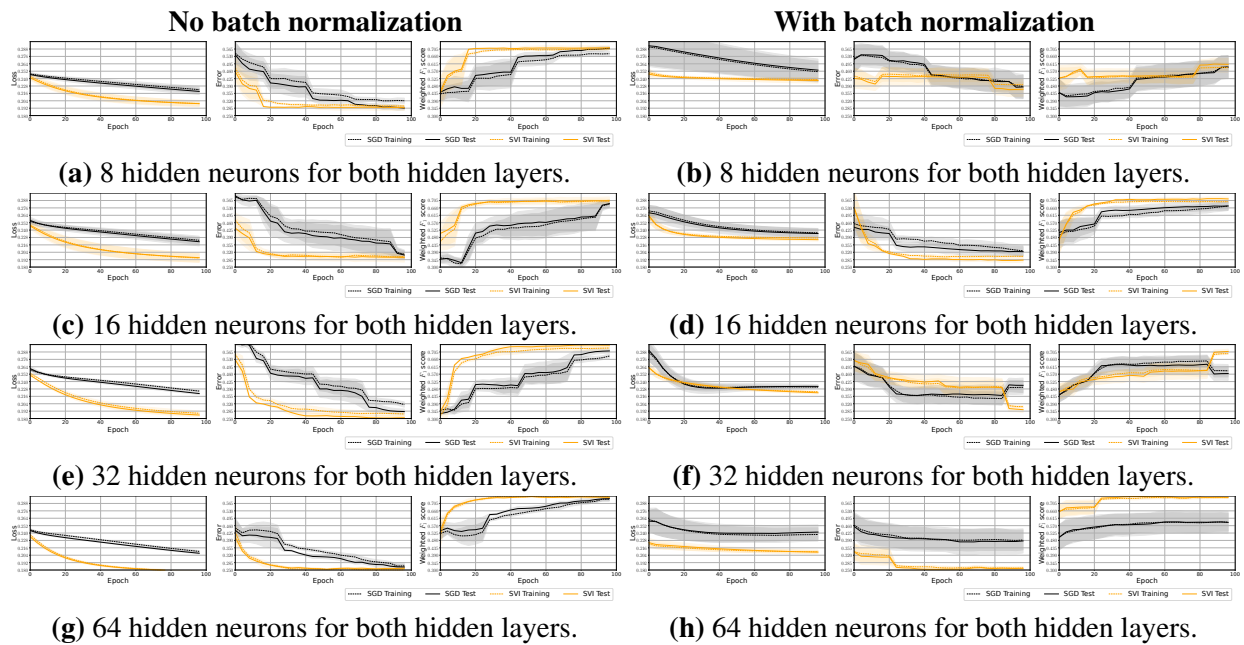
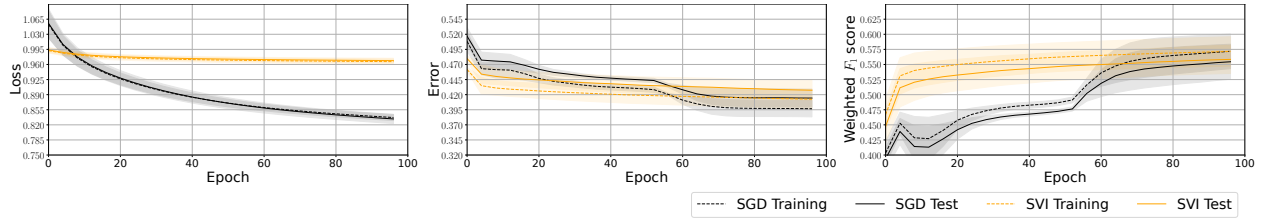
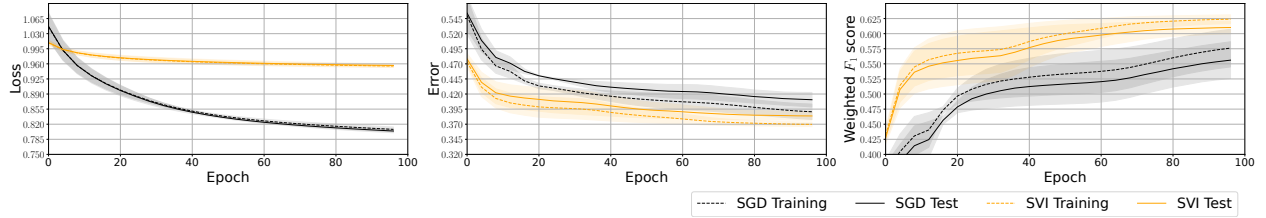


Figure 16: Los Angeles solar binary ramping event detection under a three-layer GCN model. Left to right in each three-column figure: MSE loss, classification error, and weighted F_1 score. The overall pattern is similar to that in Figure 15.

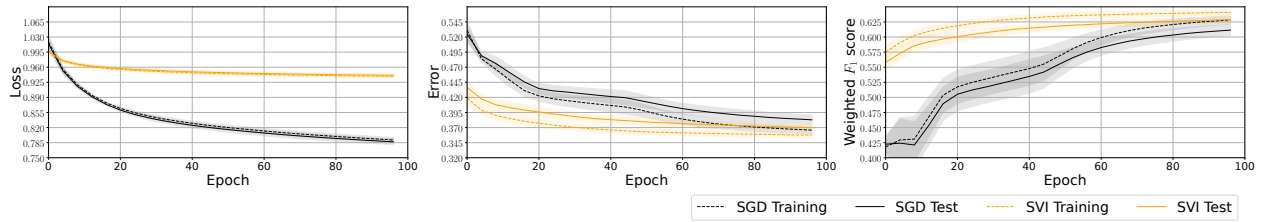
Traffic data. Data are retrieved from <https://pems.dot.ca.gov/>.



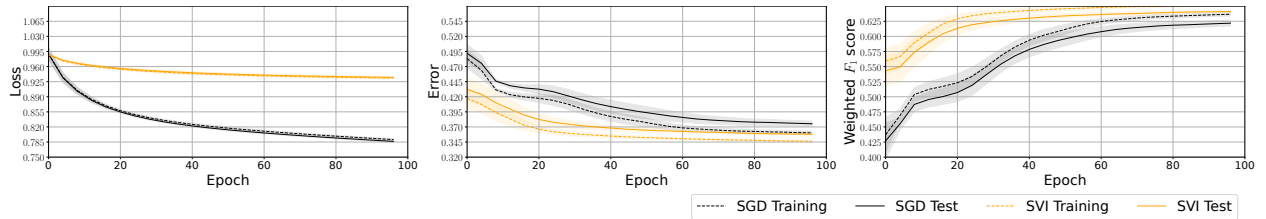
(a) 8 Hidden neurons for both hidden layers. Left to right: cross-entropy loss, classification error, and weighted F_1 score.



(b) 16 Hidden neurons for both hidden layers. Left to right: cross-entropy loss, classification error, and weighted F_1 score.



(c) 32 Hidden neurons for both hidden layers. Left to right: cross-entropy loss, classification error, and weighted F_1 score.



(d) 64 Hidden neurons for both hidden layers. Left to right: cross-entropy loss, classification error, and weighted F_1 score.

Figure 17: Traffic data multi-class anomaly detection under a three-layer GCN model. SVI shows faster convergence in terms of classification error and weighted F_1 scores. It reaches larger cross-entropy losses, which we think are benign (see Section 5.4 for justification).

B.4 Three-layer GCN model recovery and additional results

In this section, we first show the sensitivity of SVI and SGD under different batch sizes, without and without BN (see Tables 10 and 11 for final results, as well as Figure 18 and 19 for intermediate convergence). Then, we show additional results where the cross-entropy error defined in (13) is used as the training objective under the SoftPLUS activation (see Figure 20). Our goal is to show the robustness of SVI under these alternative choices. Lastly, we repeat the above additional results but replace SGD with Adam (Kingma &

Ba, 2015) (see Figure 21).

Same as we did in Appendix B.2, we now present a detailed qualitative analyses of Tables 10 (no BN, final results) and 11 (best of three, final results), as well as Figures 18 and 19 regarding intermediate convergence.

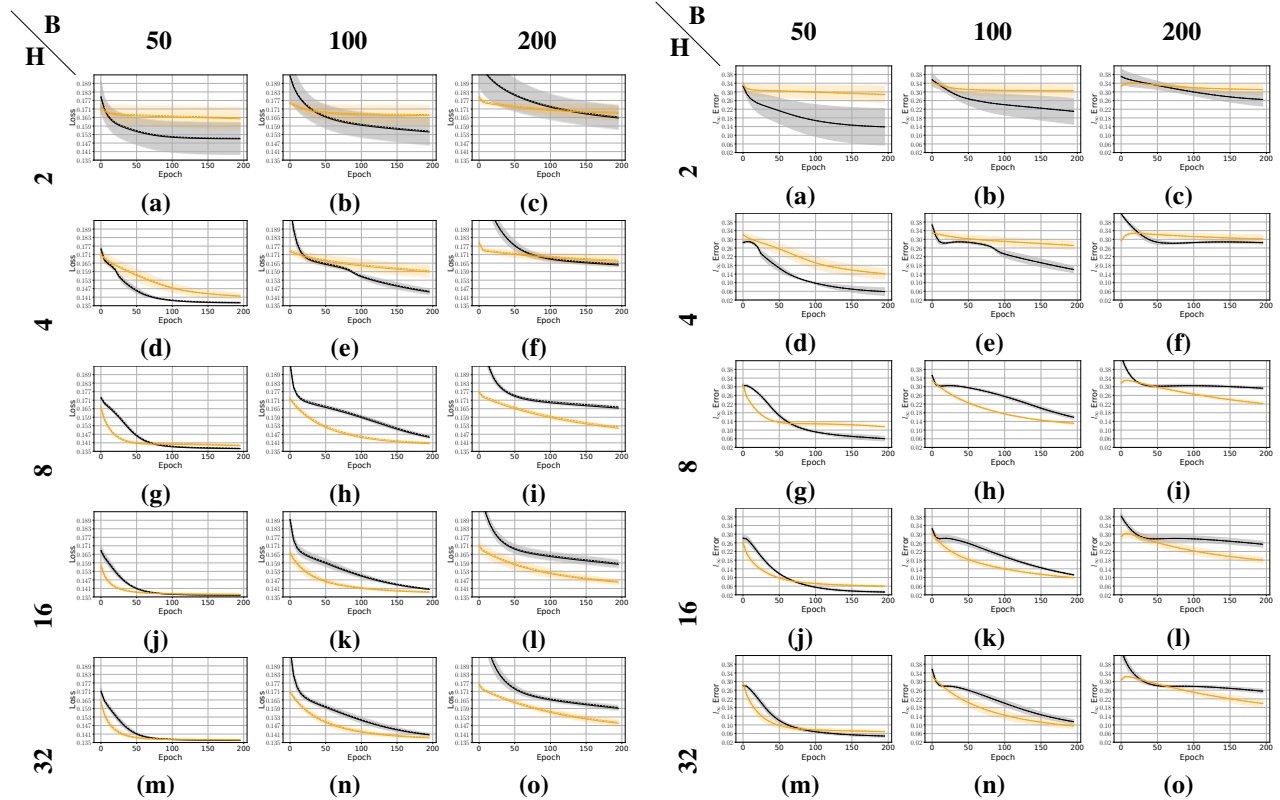
- In terms of the final MSE loss:
 - (1) when no BN is used, SVI yields smaller or nearly identical loss than SGD when $H >= 8$.
 - (2) When the best of three is chosen, SVI always has a competitive or larger loss than SGD.
- In terms of the final ℓ_∞ error:
 - (1) when no BN is used, SVI yields significantly smaller or nearly identical loss than SGD when $H >= 8$ and $B = 100$ or 200 . SVI losses are much higher when $B = 50$ regardless of H . At the same H , SVI yields higher losses as B grows. In general, SVI with $H = 16, B = 50$ reaches the fourth-smallest loss among all combinations.
 - (2) when the best of three is chosen, SVI is uniformly worse than SGD, but SVI with $H = 16, B = 50$ still reaches the fourth-smallest loss among all combinations.
- In terms of the intermediate convergence, SVI almost always reaches much lower MSE loss or ℓ_∞ error than SGD at first few epochs. In particular, running SVI for one epoch may already yield very small loss or error compared to SGD.

H	$B = 50$				$B = 100$				$B = 200$				$B = 50$				$B = 100$				$B = 200$							
	MSE loss		MSE loss		MSE loss		MSE loss		MSE loss		MSE loss		MSE loss		ℓ_∞ model recovery error		ℓ_∞ model recovery error		ℓ_∞ model recovery error		ℓ_∞ model recovery error		ℓ_∞ model recovery error		ℓ_∞ model recovery error			
	SGD train	SGD test	SVI train	SVI test	SGD train	SGD test	SVI train	SVI test	SGD train	SGD test	SVI train	SVI test	SGD train	SGD test	SVI train	SVI test	SGD train	SGD test	SVI train	SVI test	SGD train	SGD test	SVI train	SVI test	SGD train	SGD test	SVI train	SVI test
2	0.1504 (1.1e-02)	0.1500 (1.1e-02)	0.1648 (8.0e-03)	0.1641 (7.8e-03)	0.1555 (9.5e-03)	0.1548 (9.5e-03)	0.1671 (6.8e-03)	0.1663 (6.7e-03)	0.1654 (8.2e-03)	0.1647 (8.2e-03)	0.1688 (5.6e-03)	0.1680 (5.5e-03)	0.1389 (8.4e-02)	0.1388 (8.4e-02)	0.2890 (3.9e-02)	0.2878 (3.9e-02)	0.2107 (5.9e-02)	0.2102 (5.9e-02)	0.3061 (2.7e-02)	0.3051 (2.7e-02)	0.2653 (3.1e-02)	0.2647 (3.1e-02)	0.3107 (2.3e-02)	0.3104 (2.3e-02)				
4	0.1373 (6.3e-04)	0.1370 (4.2e-04)	0.1417 (2.1e-03)	0.1418 (2.1e-03)	0.1452 (1.7e-03)	0.1447 (1.8e-03)	0.1596 (3.9e-03)	0.1588 (4.1e-03)	0.1643 (1.5e-03)	0.1637 (1.4e-03)	0.1671 (3.7e-03)	0.1663 (3.9e-03)	0.0589 (1.7e-02)	0.0587 (1.7e-02)	0.1412 (2.4e-02)	0.1405 (2.5e-02)	0.1607 (1.4e-02)	0.1608 (1.4e-02)	0.2717 (2.0e-02)	0.2716 (2.0e-02)	0.2844 (6.2e-03)	0.2845 (6.1e-03)	0.3022 (1.8e-02)	0.3021 (1.8e-02)				
8	0.1371 (2.4e-04)	0.1369 (3.0e-04)	0.1393 (4.4e-04)	0.1389 (3.1e-04)	0.1455 (9.4e-04)	0.1449 (1.0e-03)	0.1411 (5.4e-04)	0.1404 (3.5e-04)	0.1662 (1.1e-03)	0.1654 (1.1e-03)	0.1522 (8.8e-04)	0.1513 (9.7e-04)	0.0601 (1.1e-02)	0.0601 (1.1e-02)	0.1162 (3.6e-03)	0.1153 (3.6e-03)	0.1591 (8.4e-03)	0.1594 (8.4e-03)	0.1315 (5.1e-03)	0.1312 (4.9e-03)	0.2932 (5.5e-03)	0.2929 (5.5e-03)	0.2225 (5.6e-03)	0.2220 (5.7e-03)				
16	0.1364 (1.3e-04)	0.1363 (7.1e-05)	0.1369 (2.6e-04)	0.1368 (8.2e-05)	0.1407 (3.1e-04)	0.1403 (3.5e-04)	0.1386 (4.6e-04)	0.1383 (3.3e-04)	0.1587 (2.6e-03)	0.1580 (2.5e-03)	0.1460 (1.6e-03)	0.1454 (1.8e-03)	0.0333 (4.1e-03)	0.0328 (4.1e-03)	0.0599 (4.0e-03)	0.0594 (4.1e-03)	0.1120 (3.7e-03)	0.1123 (3.7e-03)	0.0987 (6.1e-03)	0.0990 (6.1e-03)	0.2532 (1.4e-02)	0.2532 (1.3e-02)	0.1798 (1.3e-02)	0.1801 (1.3e-02)				
32	0.1367 (2.4e-04)	0.1365 (6.3e-05)	0.1371 (4.4e-05)	0.1368 (1.8e-04)	0.1407 (1.0e-03)	0.1404 (8.6e-04)	0.1388 (5.4e-04)	0.1383 (6.3e-04)	0.1597 (1.8e-03)	0.1590 (1.7e-03)	0.1493 (2.2e-03)	0.1485 (2.2e-03)	0.0489 (5.6e-03)	0.0486 (5.6e-03)	0.0690 (6.0e-03)	0.0685 (6.2e-03)	0.1147 (9.6e-03)	0.1150 (9.7e-03)	0.0954 (1.2e-02)	0.0953 (1.2e-02)	0.2555 (9.6e-03)	0.2556 (9.4e-03)	0.1987 (1.9e-02)	0.1987 (1.9e-02)				

Table 10: Three-layer GCN model recovery and prediction without BN at the end of epochs. See the bullet points above for detailed qualitative analyses. Metrics are defined in (12) and (16) respectively

H	$B = 50$				$B = 100$				$B = 200$				$B = 50$				$B = 100$				$B = 200$											
	MSE loss				MSE loss				MSE loss				ℓ_∞ model recovery error				ℓ_∞ model recovery error				ℓ_∞ model recovery error											
	SGD train	SGD test	SVI train	SVI test	SGD train	SGD test	SVI train	SVI test	SGD train	SGD test	SVI train	SVI test	SGD train	SGD test	SVI train	SVI test	SGD train	SGD test	SVI train	SVI test	SGD train	SGD test	SVI train	SVI test	SGD train	SGD test	SVI train	SVI test	SGD train	SGD test	SVI train	SVI test
2	0.1376 (6.3e-04)	0.1376 (4.2e-04)	0.1648 (8.0e-03)	0.1641 (2.1e-03)	0.1403 (1.1e-03)	0.1403 (1.1e-03)	0.1669 (7.5e-03)	0.1662 (7.4e-03)	0.1445 (7.1e-04)	0.1442 (6.3e-04)	0.1670 (6.3e-03)	0.1663 (5.3e-03)	0.0806 (1.7e-02)	0.0787 (1.7e-02)	0.2890 (3.9e-02)	0.2878 (3.9e-02)	0.1272 (1.6e-02)	0.1265 (1.6e-02)	0.3015 (3.2e-02)	0.3003 (3.3e-02)	0.1720 (2.0e-02)	0.1713 (2.0e-02)	0.3018 (3.2e-02)	0.3006 (3.2e-02)	0.1720 (2.0e-02)	0.1713 (2.0e-02)	0.3018 (3.2e-02)	0.3006 (3.2e-02)	0.1720 (2.0e-02)	0.1713 (2.0e-02)	0.3018 (3.2e-02)	0.3006 (3.2e-02)
4	0.1373 (6.3e-04)	0.1370 (4.2e-04)	0.1417 (8.0e-03)	0.1418 (2.1e-03)	0.1391 (5.6e-04)	0.1391 (4.4e-04)	0.1526 (5.0e-03)	0.1519 (5.0e-03)	0.1424 (1.7e-03)	0.1420 (1.5e-03)	0.1550 (5.3e-03)	0.1542 (5.3e-03)	0.0589 (2.2e-02)	0.0587 (1.7e-02)	0.1412 (2.4e-02)	0.1405 (2.5e-02)	0.1197 (8.6e-03)	0.1196 (8.5e-03)	0.2461 (2.8e-02)	0.2467 (2.8e-02)	0.1533 (2.0e-02)	0.1527 (2.0e-02)	0.2650 (2.7e-02)	0.2652 (2.7e-02)	0.1533 (2.0e-02)	0.1527 (2.0e-02)	0.2650 (2.7e-02)	0.2652 (2.7e-02)	0.1533 (2.0e-02)	0.1527 (2.0e-02)	0.2650 (2.7e-02)	0.2652 (2.7e-02)
8	0.1371 (2.4e-04)	0.1369 (3.0e-04)	0.1393 (4.4e-04)	0.1389 (3.1e-04)	0.1379 (4.5e-04)	0.1380 (3.7e-04)	0.1407 (5.0e-04)	0.1404 (6.0e-04)	0.1380 (4.5e-04)	0.1379 (3.0e-04)	0.1421 (3.4e-04)	0.1417 (2.1e-04)	0.0601 (1.1e-02)	0.0601 (1.1e-02)	0.1162 (3.6e-03)	0.1153 (3.6e-03)	0.0989 (9.9e-03)	0.0985 (1.0e-02)	0.1315 (5.1e-03)	0.1312 (4.9e-03)	0.0972 (9.3e-03)	0.0966 (9.0e-03)	0.1631 (3.5e-03)	0.1620 (2.9e-03)	0.0972 (9.3e-03)	0.0966 (9.0e-03)	0.1631 (3.5e-03)	0.1620 (2.9e-03)	0.0972 (9.3e-03)	0.0966 (9.0e-03)	0.1631 (3.5e-03)	0.1620 (2.9e-03)
16	0.1364 (1.3e-04)	0.1363 (7.1e-05)	0.1369 (2.6e-04)	0.1368 (8.2e-05)	0.1370 (9.3e-05)	0.1372 (1.8e-04)	0.1386 (4.6e-04)	0.1383 (3.3e-04)	0.1372 (1.6e-04)	0.1372 (1.9e-04)	0.1402 (3.5e-04)	0.1402 (6.0e-04)	0.0333 (4.1e-03)	0.0328 (4.1e-03)	0.0599 (4.0e-03)	0.0594 (4.1e-03)	0.0674 (4.0e-03)	0.0674 (3.7e-03)	0.0987 (6.1e-03)	0.0990 (6.1e-03)	0.0703 (5.5e-03)	0.0697 (5.5e-03)	0.1434 (8.1e-03)	0.1429 (8.6e-03)	0.0703 (5.5e-03)	0.0697 (5.5e-03)	0.1434 (8.1e-03)	0.1429 (8.6e-03)	0.0703 (5.5e-03)	0.0697 (5.5e-03)	0.1434 (8.1e-03)	0.1429 (8.6e-03)
32	0.1366 (1.1e-04)	0.1365 (6.3e-05)	0.1371 (4.4e-04)	0.1368 (1.8e-04)	0.1368 (1.7e-04)	0.1371 (1.0e-04)	0.1388 (5.4e-04)	0.1383 (6.3e-04)	0.1369 (1.8e-04)	0.1371 (2.3e-04)	0.1390 (4.6e-04)	0.1389 (1.5e-04)	0.0489 (5.6e-03)	0.0486 (5.6e-03)	0.0690 (6.0e-03)	0.0685 (6.2e-03)	0.0663 (1.9e-03)	0.0662 (1.9e-03)	0.0954 (1.2e-02)	0.0953 (1.2e-02)	0.0636 (1.9e-03)	0.0652 (1.7e-03)	0.1199 (1.7e-03)	0.1205 (1.9e-03)	0.0636 (1.9e-03)	0.0652 (1.7e-03)	0.1199 (1.7e-03)	0.1205 (1.9e-03)	0.0636 (1.9e-03)	0.0652 (1.7e-03)	0.1199 (1.7e-03)	0.1205 (1.9e-03)

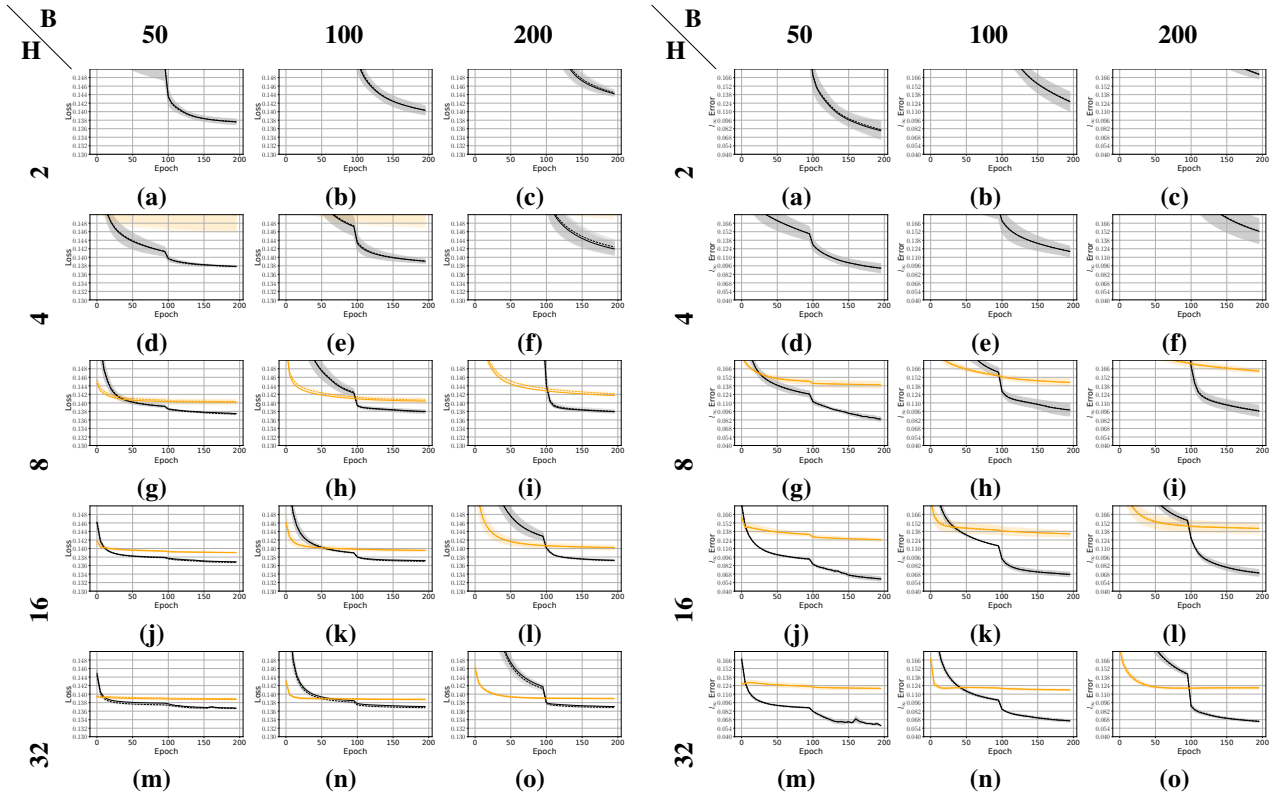
Table 11: Three-layer GCN model recovery and prediction for the best-of-three result at the end of epochs. See the bullet points before Table 7 for detailed qualitative analyses. Metrics are defined in (12) and (16) respectively.



MSE loss by H and B . The metric is defined in (12). Black (orange) solid (dash) lines denote SGD (SVI) test (training) results.

ℓ_∞ error by H and B . The metric is defined in (16). Black (orange) solid (dash) lines denote SGD (SVI) test (training) results.

Figure 18: Three-layer GCN model recovery and prediction without BN regarding intermediate convergence. See the bullet points before Table 10 for detailed qualitative analyses. Some curves miss initial values because they are too large under the shared y-ticks. Metrics are defined in (12) and (16) respectively.

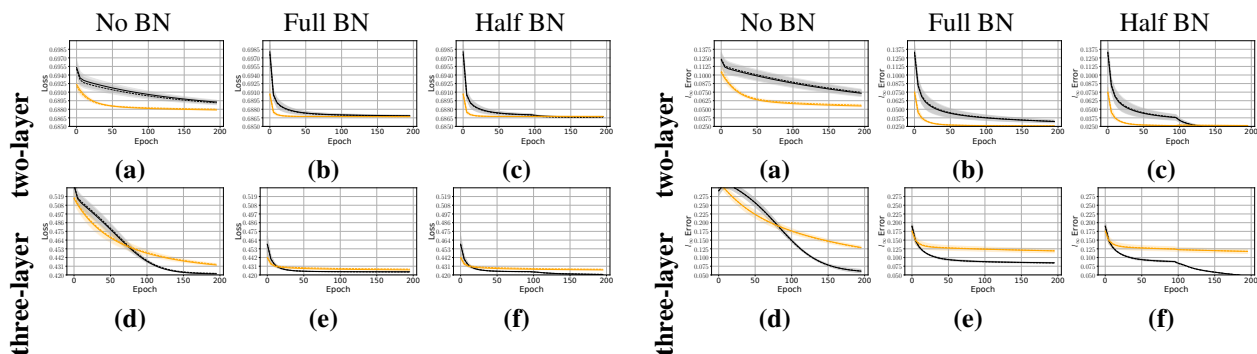


MSE loss by H and B . The metric is defined in (12). Black (orange) solid (dash) lines denote SGD (SVI) test (training) results.

ℓ_∞ model recovery error by H and B . The metric is defined in (16). Black (orange) solid (dash) lines denote SGD (SVI) test (training) results.

Figure 19: Three-layer GCN model recovery and prediction under half-frozen BN regarding intermediate convergence. We found that half-frozen BN generally further accelerates BN. See the bullet points before Table 10 for detailed qualitative analyses. Some curves miss initial values because they are too large under the shared y-ticks. Metrics are defined in (12) and (16) respectively.

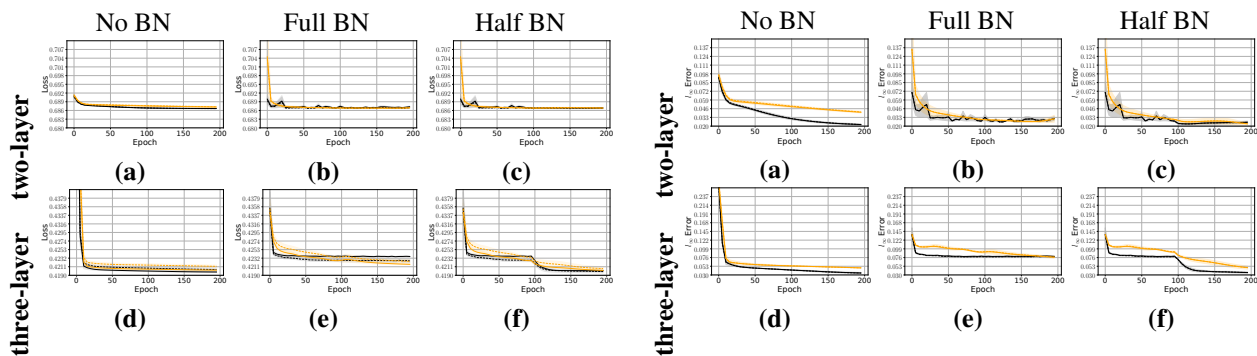
In addition to comparing SGD vs. SVI under MSE loss and the ReLU activation, we also compare both under the cross-entropy loss and the SoftPLUS activation, where the β parameter is chosen as 5, tuned after normalization (see Figure 20). We do so to show the robustness of SVI. We also compare Adam with SVI under this additional setting (see Figure 21). For SGD vs. SVI, the pattern is consistent with earlier findings. For Adam vs. SVI, Adam under no BN performs better than SVI, likely because the gradient normalization steps in Adam are not directly applicable to SVI, which does not use gradients. Under full BN, it is interesting that SVI performs very similarly to Adam, a phenomenon that we will explore more in the future. Under half BN, the comparison between Adam and SVI is very similar to that between SGD and SVI.



MSE loss by H and B . The metric is defined in (12). Black (orange) solid (dash) lines denote SGD (SVI) test (training) results.

ℓ_∞ model recovery error by H and B . The metric is defined in (16). Black (orange) solid (dash) lines denote SGD (SVI) test (training) results.

Figure 20: SGD vs. SVI under the SoftPLUS activation and the cross-entropy loss, with $H = 16$ and $B = 100$. The overall pattern is similar as before, so that SVI is robust under alternative loss and activation functions.



MSE loss by H and B . The metric is defined in (12). Black (orange) solid (dash) lines denote Adam (SVI) test (training) results.

ℓ_∞ model recovery error by H and B . The metric is defined in (16). Black (orange) solid (dash) lines denote Adam (SVI) test (training) results.

Figure 21: Adam vs. SVI under the SoftPLUS activation and the cross-entropy loss, with $H = 16$ and $B = 100$. The overall pattern is similar as before, where the gap between SVI and Adam is smaller than that between SVI and SGD under BN for three-layer GCN.

B.5 Four-layer OGB real-data

We conduct further experiments when the number of hidden neurons in each hidden layer is reduced to 128 or 256. Figure 22 shows improved initial convergence by SVI or SVI-Adam over the competitors, a pattern consistently observed earlier, and competitive overall accuracies. In particular, SVI is consistent under different number of hidden neurons whereas SGD performs clearly worse under 128 hidden neurons.

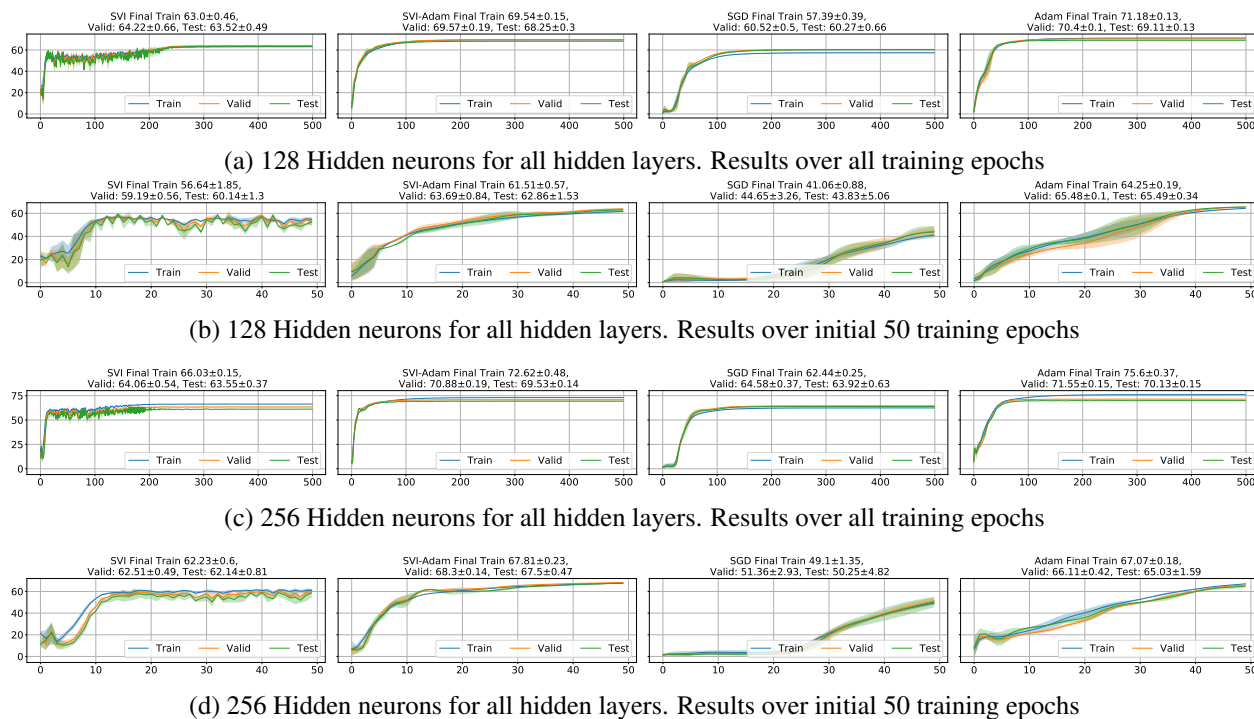


Figure 22: OGB large-scale real-data example under either 128 or 256 hidden neurons for all hidden layers. The setup is identical to Figure 6. It is clear that SVI or SVI-Adam still exhibits comparable final accuracy and improved convergence at initial training stages under such variants. In particular, SGD is sensitive to the number of hidden neurons, as its final accuracies under 128 hidden neurons are clearly poorer than those by SVI and very different from SGD performance under 256 hidden neurons. In contrast, SVI or SVI-Adam performs more consistently.